Applied Energy 211 (2018) 492–512

Contents lists available at ScienceDirect

Applied Energy

journal homepage: www.elsevier.com/locate/apenergy

An analysis-forecast system for uncertainty modeling of wind speed: A case study of large-scale wind farms

Jianzhou Wang[a], Tong Niu[a,*], Haiyan Lu[b], Zhenhai Guo[c], Wendong Yang[a], Pei Du[a]

[a] School of Statistics, Dongbei University of Finance and Economics, Dalian 116025, China
[b] Department of Software Engineering, University of Technology, Sydney, Australia
[c] State Key Laboratory of Numerical Modelling for Atmospheric Sciences and Geophysical Fluid Dynamics, Institute of Atmospheric Physics, Chinese Academy of Sciences, Beijing 100029, China

HIGHLIGHTS

- An analysis-forecast system for wind speed uncertainty modeling is proposed.
- Recurrence analysis is developed to study the characteristics of wind speed.
- Feature selection is developed to determine optimal system input.
- An improved multi-objective optimizer is first proposed to optimize the system further.
- The proposed system shows a greater advantage over benchmark models considered.

ARTICLE INFO

Keywords:
Analysis-forecast system
Chaos technique
Multi-objective optimization algorithm
Feature selection
Wind speed series

ABSTRACT

The uncertainty analysis and modeling of wind speed, which has an essential influence on wind power systems, is consistently considered a challenging task. However, most investigations thus far were focused mainly on point forecasts, which in reality cannot facilitate quantitative characterization of the endogenous uncertainty involved. An analysis-forecast system that includes an analysis module and a forecast module and can provide appropriate scenarios for the dispatching and scheduling of a power system is devised in this study; this system superior to those presented in previous studies. In order to qualitatively and quantitatively investigate the uncertainty of wind speed, recurrence analysis techniques are effectively developed for application in the analysis module. Furthermore, in order to quantify the uncertainty accurately, a novel architecture aimed at uncertainty mining is devised for the forecast module, where a non-parametric model optimized by an improved multi-objective water cycle algorithm is considered a predictor for producing intervals for each mode component after feature selection. The results of extensive in-depth experiments show that the devised system is not only superior to the considered benchmark models, but also has good potential practical applications in wind power systems.

1. Introduction

In recent years, given its advantages, such as renewability and cleanness, the comprehensive exploitation and utilization of wind energy has made it extensively socially and economically effective. More importantly, it is self-evident in a comparison of wind energy and conventional energy, which is a significant cause of global warming and atmospheric contamination, that wind power is one of the most promising energy sources available worldwide. Thus, wind energy is a greatly preferred energy resource in many parts of the world [1]. For example, wind power may become the second largest resource for generating electricity in China by 2050 [2]. However, in practice, the efficient and comprehensive development of wind power systems is considerably restricted because of the intrinsic randomness and intermittency of wind speed, which presents a significant challenge in terms of electrical network operation and management, in particular wind power integration (WPI). Accordingly, the effective analysis and accurate forecasting of wind speed not only constitute a challenging task, but are also an emphatic concern for those who make decisions-related to wind farms. It is crucial both to design more appropriate and efficient wind farms and to further determine the nonlinear dynamic pattern of wind speed in order to better manage and minimize the operational risks.

The analysis and investigation of the dynamic characteristics, in

* Corresponding author at: School of Statistics, Dongbei University of Finance and Economics, Shahekou district, Dalian 116025, Liaoning Province, China.
E-mail address: niuchenren621@126.com (T. Niu).

https://doi.org/10.1016/j.apenergy.2017.11.071
Received 25 July 2017; Received in revised form 3 November 2017; Accepted 13 November 2017
Available online 20 November 2017
0306-2619/

Nomenclature

WPI	wind power integration
WSFM	wind speed forecast model
WSF	wind speed forecast
AR	autoregressive model
ARIMA	autoregressive integrated moving average model
ARCH	autoregressive conditional heteroskedasticity model
ANNs	artificial neural networks
PSO	particle swarm optimization
GA	genetic algorithm
LUBE	lower upper bound estimation
ELM	extreme learning machine
LLFNN	local linear fuzzy neural network
RBFNN	radial basis function neural network
WNN	wavelet neural network
MIMO-LSSVM	multi-input multi-output least squares support vector machine
WCA	water cycle algorithm
IMOWCA	improved multi-objective water cycle algorithm
EMD	empirical mode decomposition
EEMD	ensemble empirical mode decomposition
CEEMD	complete ensemble empirical mode decomposition
CEEMDAN	complete ensemble empirical mode decomposition with adaptive noise
IMFs	intrinsic mode functions
MIMO-LSSVM	multi-input multi-output least squares support vector machine
WCA	water cycle algorithm
RR	recurrence rate
DET	determinism
ENTR	entropy
L	average diagonal line length
$\vec{\mathbf{X}}^{i}_{River}$	the position of river
$\vec{\mathbf{X}}^{i}_{Sea}$	the position of sea
RR	recurrence rate
DET	determinism
ENTR	entropy
$\vec{\mathbf{X}}^{i}_{Stream}$	the position of stream
Randn	an uniformly distributed random numbers in [1,1]
C	a constant in Eqs. (13)–(15) and (21)
z_i	actual observed value of wind speed
τ	delay time
m	embedding dimension
ϖ	time window
$\|\cdot\|$	a norm
diag	diagonal matrix
LB	lower bound of variables
UB	upper bound of variables
max_iteration	maximum iteration number
ω	adaptive inertia weight
GD	generational distance
SP	spacing
CP	coverage probability
AW	average width
AWD	accumulated width deviation
$\boldsymbol{L}_i$	lower bound of *i-th* prediction interval
$\boldsymbol{U}_i$	upper bound of *i-th* prediction interval
c_i	a Boolean value
ς	predefined threshold in recurrence analysis
$P(l)$	the probability to find a diagonal line of length l in the recurrence plot
$\Phi(\cdot)/\boldsymbol{\phi}(\cdot)$	the nonlinear mapping
$\boldsymbol{\alpha}$	interval width coefficient
$\boldsymbol{I}_i$	the *i*-th prediction interval
rand	a uniformly distributed random number in [0,1]
Nsr	the number of streams
Npop	the number of raindrops
d_{max}	a small number close to zero
$\boldsymbol{\Theta}(\cdot)$	heavisible function
Costn	the fitness value of the *n*-th raindrop
$\boldsymbol{T}$	training dataset
MLYE	maximum lyapunov exponent
d_{max}	the tolerance in IMOWCA
Std.	standard deviation
$S(t)_{mean}$	a statistic shown in Eq. (7)
$\Delta S(t)_{mean}$	a statistic shown in Eq. (8)
$Scor(t)$	a statistic shown in Eq. (9)
$\mathscr{R}^p$	input space with the dimension of p
MLYE	maximum lyapunov exponent

particular the predictability, of nonlinear systems are important for forecast modeling. However, most of the studies in the literature placed emphasis mainly on certain basic statistics, such as the maximum, minimum, average, and standard deviation [3,4]. Further, the Lyapunov exponent, complexity, skewness, kurtosis, and emergence of wind speed were investigated in Ref. [5]. Effective studies on the statistical distribution of wind speed, which is usually assumed to be a Weibull distribution function, in order to further determine wind speed patterns were reported in Refs. [6–8]. Evidently, these statistics do not suffice to reveal the profound characteristics of complex nonlinear systems, in particular highly volatile wind speed series. The recurrence plot and recurrence quantification analysis, which is essentially based on chaos theory, as an effective technique for studying complicated nonlinear systems, were developed in the field of wind speed forecasting. In the study reported in Ref. [9], wind speed series were analyzed using recurrence plots. However, this analysis was limited to recurrence plots, and is still not sufficient to quantitatively investigate the system behaviors of wind speed series. In order to further remedy the defect of recurrence plots that they lack quantitative analyses, a recurrence quantification analysis of recurrence plots, which can also be used to visualize the trajectories in phase space, was effectively developed in this study in order to investigate in greater depth the dynamic characteristics and predictability of wind speed series and the corresponding mode components.

Accurate modeling of wind speed has important practical significance for wind energy development and utilization in many forms, such as wind turbines that convert wind power into kinetic energy and mean flow acoustic engines that convert the mean flow power into acoustic power [10–12]. However, given the complex dynamic pattern of wind speed, the design of an effective and scientific wind speed forecast model (WSFM) is consistently attracting considerable research attention. In general, the mainstream studies of WSFMs can be systematically categorized into those using physics and statistical approaches [13] and artificial intelligence methods. Rich physics models involving wind speed forecasts (WSFs) were systematically introduced in Refs. [14–18]. Technically, these models in general involve computational fluid dynamics in order to simulate the atmosphere based on different grid designs [13]. In contrast to physics models, the alternative WSFMs are based on statistical modeling and machine learning theories, which are convenient for implementing the modeling and simulation of wind speed forecasting because of their accessibility and excellent local prediction ability. In earlier research on WSFMs, the traditional statistical models, which usually consist of an autoregressive model (AR) [19], autoregressive integrated moving average model

(ARIMA) [20,21], fractional-ARIMA [22], or autoregressive conditional heteroskedasticity model (ARIMA-ARCH) [23], played a widespread role in the WSF field. In recent years, forecast models based on machine learning theories, in particular artificial neural networks (ANNs), have become popular in the WSF field. In general, they are trained using the historical information of wind speed in order to establish nonlinear mapping between the input set and target set. Theoretically, the self-learning and self-organizing capabilities of ANNs are excellent and therefore, considerable effort has been invested by many researchers in ANNs for use in WSF [24–26]. However, the effectiveness and efficiency of hybrid models in general makes them superior to single neural network models in terms of achieving accurate WSFs. As a consequence, many studies on hybrid forecast models have been reported every year. Most of these models usually focused attention on data preprocessing [27–30] and model parameter optimization using heuristic algorithms, such as the particle swarm optimization (PSO) [31,32], and genetic algorithms (GAs) [31,33–35].

In addition to wind speed forecasting, reliable wind power forecasting plays an important role in the scheduling and operation of wind farm power systems. Many scholars have invested effort in the study of accurate wind power forecasting using models-based machine learning theory. In [36], an adaptive network-based fuzzy inference system, which incorporated a wavelet and a PSO algorithm, was developed to achieve short-term wind power forecasting. A hybrid forecasting model, combining a support vector machine (SVM) and a Markov model, was proposed in [37] to achieve wind power forecasting. In [38], a random forests model was proposed, aimed at performing one hour ahead wind power forecasting. ANNs with self-learning and generalization capabilities have been widely applied in the field of wind power forecasting. In [39], a bidirectional mechanism using an extreme learning machine (ELM), a well-known ANN model, was established for wind power forecasting. In order to achieve accurate wind power forecasting, an effective forecasting framework, including a local linear fuzzy neural network (LLFNN) optimized by a seeker optimization algorithm, discrete wavelet transform, and singular spectrum analysis, was proposed in [40]. In [40], a forecasting model based on chaotic time series was presented for wind power forecasting, where phase space reconstruction and a Bernstein neural network were combined. Additionally, effort was invested in wind power forecasting using a radial basis function neural network (RBFNN) [41] and wavelet neural network (WNN) [42] with the aim of achieving accurate wind power forecasting results.

Most of the aforementioned studies were focused mainly on point forecasts, which cannot easily quantify uncertain information in the process of wind speed forecasting. However, the study of the interval prediction of wind speed or wind power has not received sufficient attention, despite its significance to the risk management, power dispatching and WPI of wind farms. In practical power grid management, uncertainty analysis and mining is beneficial for ameliorating the adverse effects of the stochastic volatility of wind speed and for effectively providing more comprehensive reference information to operational risk decision makers. For this reason, uncertainty modeling is becoming a prevailing research direction of many scholars in this field of the study. However, the study of uncertainty modeling is still in its infancy. Currently, there are only a few studies on uncertainty quantification, and the mainstream research direction relies largely on statistic methods, including quantile regression [43–45], bootstrap methods [46], and kernel density estimation [47]. Additionally, an interval prediction method using nonparametric theory, lower upper bound estimation (LUBE), based on ANNs was proposed to construct prediction intervals [48].

A comprehensive evaluation of the forecasting models for wind speed and wind power mentioned above was conducted in this study; the results are summarized in Table 1. In point forecasting models, the application of physics models is significantly restricted because of the complex meteorological conditions, model initialization, and heavy computation cost, despite their excellent long-term forecasting capabilities. The computation efficiency of conventional statistical models, including AR, ARIMA, and so forth, is high. However, their linear form restricts their ability to model accurately nonlinear time series, such as wind speed and wind energy time series. A key problem related to ANNs is that they are easily trapped in local optimization, although they have excellent capabilities for modeling nonlinear time series. Furthermore, in the field of interval prediction, research is focused on quantile regression because of its particular advantages, shown in Table 1. However, the main drawback of quantile regression methods is that it is necessary to acquire a particular training dataset to establish a forecast model when using the method to develop prediction intervals. Additionally, in quantile regression each quantile needs to be modeled, which increases not only the computational burden but also the probability of results being discarded in the resampling process [49]. The bootstrap method is a statistical method that uses data resampling with replacement to estimate the robust properties of almost any statistics, such as standard errors, some parameters of confidence intervals, and the coefficients of correlation and regression [50]. Bootstrap methods can avoid the possible drawbacks of the quantile regression method. However, they are only very effective when addressing small sample sizes and thus their application is restricted when addressing a large-scale sample set. Kernel density estimation, which can construct

Table 1
Evaluation of forecasting models including point and interval prediction.

Category	Model	Merit	Demerit
Point prediction	Physics models	Good space-time continuum; high temporal and spatial resolution; clear physics process; long-term forecasting	Complex modeling process; heavy computational burden; poor local predictability; large forecasting error resulting from complex meteorological conditions and model initialization
	Statistical models (AR, ARIMA, ARIMA-GRCH, fractional-ARIMA.)	High computation efficiency; less model parameters to be tuned; good predictive performance for linear data	Poor prediction accuracy for nonlinear data; applicable only to stable data; assume that the interference sequence is white noise
	Artificial neural network (such as WNN, RBFNN, ELM, and so forth.)	Able to approximate any nonlinear relationship theoretically; good generalization capability; excellent self-learning capability	Complex computational process; sensitive to the size of training samples; easily fall into the local optimum
Interval prediction	Quantile regression	Able to handle heterogeneity problem; not sensitive to outliers; considers the entire distribution; able to capture the tail characteristics of the distribution	Requires a specific set of training samples; heavy computational burden; the probability of results being discarded in the process of repetitive computing
	Bootstrap methods	Avoid possible discards in quantile regression; very effective when dealing with small samples	Poor performance when handling large samples; heavy computational burden
	Kernel density estimation	Easily constructs prediction interval	Strict assumptions on distribution
	LUBE	Avoids the assumptions about distribution of studied data; high computational efficiency; easily adjustable model coefficients	Complex objective function; the objective function cannot be optimized by the traditional mathematical method

prediction intervals rapidly, is based on point forecast results along with an assumed statistical, usually Gaussian, distribution of historical errors. However, the presumed error distribution does not match the actual error distribution. Accordingly, merely using Gaussian distribution to configure the error distribution is far from sufficient. Considering the aforementioned analysis, the hypothetical error distribution using Gaussian distribution may unavoidably produce the bias and risks when developing prediction intervals. As compared with traditional interval prediction models based on parameter statistics, the LUBE method avoids the restrictive distribution assumption and heavy computation burden when constructing prediction intervals. However, the objective function construction of the LUBE method is complex and cannot be optimized by using traditional mathematical methods. In this study, an improved multi-objective optimization algorithm was employed to optimize the key parameters of the LUBE method, which is an additional contribution of this study. Existing progress in WSFM using LUBE was achieved mainly with the aid of ANNs. However, ANNs are sensitive to complex training parameters and likely to become trapped in local optima. Accordingly, a robust multi-input multi-output least squares SVM (MIMOLSSVM) based on machine learning theory, which requires fewer parameters that need to be tuned than NNs, was developed in this study.

Most of the literature concerning wind speed forecasting underlines mainly data preprocessing and model optimization. The investigation of feature selection as applied in wind speed forecasting has received little attention. Feature selection, which can remove certain irrelevant features and enhance the capability of the forecasting model to learn the nonlinear relationship in time series, is an effective technique for selecting appropriate model input when performing forecasts. In previous studies in the literature, the input forms of the model usually depended on subjective experience and repeated experiments, which reduces to a certain degree the efficiency of constructing prediction intervals. The development of a feature selection technique for interval prediction models of wind speed is an important contribution of this study. Furthermore, more effort should be invested in developing feature selection for wind speed and power forecasting to improve its accuracy and efficiency further.

In consideration of the significance of nonlinear analysis and forecast modeling, a novel analysis-forecast system, combining an analysis module and a forecast module, is proposed in this paper. For the analysis module, recurrence analysis techniques based on chaos theory, including recurrence plot and recurrence quantification analysis, were effectively developed to study the dynamic behaviors and predictability of the nonlinear system based on wind speed series. For the forecast module, a novel framework of uncertainty mining was devised, which systematically combines LUBE theory, MIMOLSSVM, complete ensemble empirical mode decomposition with adaptive noise (CEEMDAN) based on mode decomposition theory, a feature selection technique using phase space reconstruction, and an improved multi-objective water cycle algorithm (IMOWCA). However, MIMOLSSVM is also sensitive to the inherent parameters, namely regularization parameter and squared kernel bandwidth parameter. IMOWCA, aimed to optimize the key parameters of the forecast module in order to strengthen the effectiveness and robustness of MIMOLSSVM, is presented for the first time in this paper. In fact, feature selection can enhance the operational efficiency by reducing the training time and improve the model generalization by avoiding over-fitting. However, in previous studies of interval prediction, the feature selection technique usually was not taken into account in the development of uncertainty modeling. In this study, a classical and effective feature selection technique based on chaos theory, the C−C method, was developed for implementing feature selection and thus obtaining the optimal input forms for MIMOLSSVM. More importantly, in order to effectively model the nonlinear system based on wind speed series, the raw wind speed series is decomposed into intrinsic mode functions (IMFs) by using the CEEMDAN method. Furthermore, in order to reduce the computation complexity, the generated IMFs are merged in accordance with the corresponding complexity degree, and then, the proposed model implements uncertainty modeling for each reconstituted IMF. Finally, the prediction intervals generated by each IMF are merged to obtain the final interval prediction results. The devised analysis-forecast system is called Modes-IMOWCA-CC-MIMOLSSVM, accordingly.

In contrast to a parametric model, the devised forecast module based on LUBE makes no assumption concerning distribution shape, and thus, uncertainty modeling is more convenient and effective. As compared to NNs, the forecast module based on MIMOLSSVM needs fewer model parameters and avoids the over-fitting problem, usually obtaining satisfactory forecast results. Phase space reconstruction based on chaos theory, which is superior to the previous feature selection methods, was developed in this study to adaptively determine the optimal input feature.

The main contributions of the devised analysis-forecast system can be summarized as follows.

(1) A novel analysis-forecast system of wind speed is proposed in this paper, aimed at improving the effectiveness of constructing effective prediction intervals to improve the management and scheduling of wind power systems.
(2) The notion of mode components was originally developed in this study with the aim of effectively performing uncertainty analysis and mining for the nonlinear system based on wind speed series, which is proved to be an effective and robust method.
(3) Importantly, the particular advantage of the devised forecast module is its simplicity, since it avoids the assumption on distribution shape, as compared to conventional parametric statistical models. This significantly reduces the complexity of uncertainty modeling and strengthens the robustness and efficiency of the system.
(4) The feature selection technique based on delayed embedding theory was developed in this study to determine the optimal input features when developing the prediction intervals, which is an important contribution of this study.
(5) Together with phase space reconstruction, the inherent trajectories of a nonlinear system based on wind speed series are determined using recurrence plots and recurrence quantification analysis, which can effectively reveal the predictability of wind speed series.
(6) IMOWCA is proposed in this paper to optimize the key parameters of the forecast module in this system. The experimental results manifest that IMOWCA outperforms its primitive in the process of constructing prediction intervals.
(7) Effective sensitivity testing, which further elucidates the robustness, effectiveness, and efficiency of the devised analysis-forecast system, is described in this paper, and extensive discussions are presented.

The remainder of this paper is organized as follows. Section 2 introduces the preliminaries of the proposed analysis-forecast system. In Section 3, the overall framework of the system is introduced. Implementations of the analysis module and forecast module to verify the effectiveness of the proposed system are described in Section 4. Further discussions about the system are presented in Section 5. Finally, the conclusion of this paper is put forth in Section 6.

2. Methodology

In this section, a modes decomposition method and recurrence analysis techniques are introduced. Furthermore, the detailed theory of feature selection using the C−C method is described. Finally, MIMOLSSVM and its optimization using IMOWCA are introduced.

2.1. Modes decomposition and recurrence analysis

Nonlinear systems, in particular wind speed series, have complex system characteristics, such as high volatility, randomness and intermittency, and thus, it is difficult to accurately model the uncertainty of wind speed series. Therefore, mode (or frequency domain) decomposition for wind speed series, which can largely reduce their complexity, must be implemented. In this section, a novel mode decomposition method, namely CEEMDAN, is briefly introduced. Additionally, considering the complexity of wind speed series, an effective frequency-time analysis module based on recurrence plots and recurrence quantification analysis is used to analyze and study the dynamic characteristics of wind speed series.

In order to effectively investigate and model the frequency components of wind speed, CEEMDAN, a powerful mode decomposition method, is applied in the devised forecast module. CEEMDAN, an advanced extension of the complementary ensemble empirical mode decomposition (CEEMD) method proposed by Yeh et al. in [51], was first presented in [52]. As compared to the previously proposed empirical mode decomposition (EMD) [53], ensemble empirical mode decomposition (EEMD) [54], and complementary ensemble empirical mode decomposition (CEEMD) methods, the distinct merits of CEEMDAN are as follows. (1) The noise coefficient vector is extended to adjust the added noise level in the process of decomposition. (2) The generated IMFs are completely reconstructed without a noise component. (3) The method is more efficient than EEMD and CEEMD. Further details concerning CEEMDAN can be found in Ref. [52].

The nonlinear systems, in particular wind speed series, show significant uncertainties, unexpected randomness, and complicated nonlinear specialties, and thus, uncertainty modeling is a challenging task. Therefore, explorations of the systematic features of nonlinear systems are always constantly in progress worldwide. Recurrence is a fundamental property of a dynamical system, which can be exploited to characterize the system's behavior in phase space [55]. In general, the recurrence phenomenon occurs in nonlinear systems, especially chaos systems, which provides an effective path for investigating the dynamic properties based on phase space constructed by the C−C method. Thus, the recurrence plot was first proposed by Eckman et al. [56] in order to effectively address the problem. The recurrence plot can be implemented via the following matrix $\mathbf{R}_{i,j}$, which can be translated into a recurrence plot.

$$\mathbf{R}_{i,j} = \mathbf{\Theta}(\varsigma - \|\vec{x}_i - \vec{x}_j\|), \quad i,j = 1,2,...,N \tag{1}$$

where $\vec{x}_i$ denotes a point in phase space, and ς and $\mathbf{\Theta}$ represent the threshold and Heaviside function, respectively. It is worth mentioning that the threshold is in general determined as 0.4–0.5 times the standard deviation of the studied wind speed data.

Table 2 [55] shows identification methods of recurrence plots and their different interpretations. In Fig. 1, an illustrative example based on the Lorentz system in order not only to visualize the recurrence plot, but also to analyze its characteristics is shown. In this example, the embedding dimension and delay time of Lorentz series (X_i,i = 1,2,...,3000) can be obtained by the C−C method mentioned below. According to the obtained embedding dimension and delay time, the Lorentz attractor can be retrieved, as shown in Fig. 1. In this figure, the recurrence plot is clearly displayed with a threshold value 0.3 for the recurrence matrix, from which the conclusion can be drawn that the analyzed system is chaotic according to the sixth identification method in Table 2.

In this study, recurrence plots, together with CEEMDAN, were used to unveil the intricate dynamic traits of a nonlinear system and visualize the trajectories existing in actual phase space. Theoretically and technically, the times when the trajectory encounters approximately the same region in phase space can be effectively identified by the recurrence plot.

Nevertheless, merely using the recurrence plot to identify the dynamic pattern of a nonlinear system is not sufficient because of the absence of a qualitative analysis. For this reason, a recurrence quantification analysis including metrics was proposed in [57–59] in order to analyze a nonlinear system from the qualitative perspective, which usually involves certain statistical standards, including recurrence rate (*RR*), determinism (*DET*), entropy (*ENTR*), and average diagonal line length (*L*). The definitions of these four metrics are described as follows.

(1) Recurrence rate (*RR*): *RR* is a metric that calculates the proportion of recurrence points corresponding to the recurrence plot, which can be utilized to uncover the system dynamics in phase space.

$$RR(\varsigma) = \frac{1}{N^2}\sum_{i,j=1}^{N} \mathbf{\Theta}(\varsigma - \|\vec{x}_i - \vec{x}_j\|), \quad i \neq j \tag{2}$$

(2) Determinism (*DET*): *DET* is the ratio of recurrence points that form diagonal structures of length at least l_{min} to all recurrence points. Theoretically, the phenomenon of no or very short diagonals occurs if the processes are uncorrelated or weakly correlated and the behavior is stochastic or chaotic, whereas a deterministic process produces longer diagonals with fewer single isolated recurrence points. Accordingly, *DET* provides an insight for investigating the determinism and the predicting capability of a system.

$$DET = \frac{\sum_{l=l_{min}}^{N} lP(l)}{\sum_{l=1}^{N} lP(l)} \tag{3}$$

where $P(l)$ is the histogram of diagonal lines of length l with the threshold ς.

(3) Average diagonal line length (*L*): *L* is the average distance between two segments of the trajectory, which can be interpreted as the mean prediction time.

$$L = \frac{\sum_{l=l_{min}}^{N} lP(l)}{\sum_{l=l_{min}}^{N} P(l)} \tag{4}$$

(4) Entropy (*ENTR*): *ENTR* refers to the Shannon entropy of the probability $p(l) = P(l)/N_l$ to find a diagonal line of exactly length l in the

Table 2
Identification approaches for recurrence plots.

Observation	Interpretation
Homogeneity	Stationary process
Fading to the upper left and lower right corners	Nonstationarity; some states are rare or escape the normal; transitions may have occurred
Tapebreak occurs	Nonstationarity; states are rare or far from the normal
Periodic or quasi-periodic patterns	Periodical process; long diagonal lines with different distances between each other reveal a quasi-periodic process
Single isolated points	Heavy fluctuation in the process; the appearance of single isolated points implies randomness in the process
Diagonal lines	Deterministic process; the evaluation of states is analogical at different times; the process is chaotic if diagonal lines occur alongside single isolated points
Vertical and horizontal lines/clusters	Weak volatility in the process; laminar states have occurred

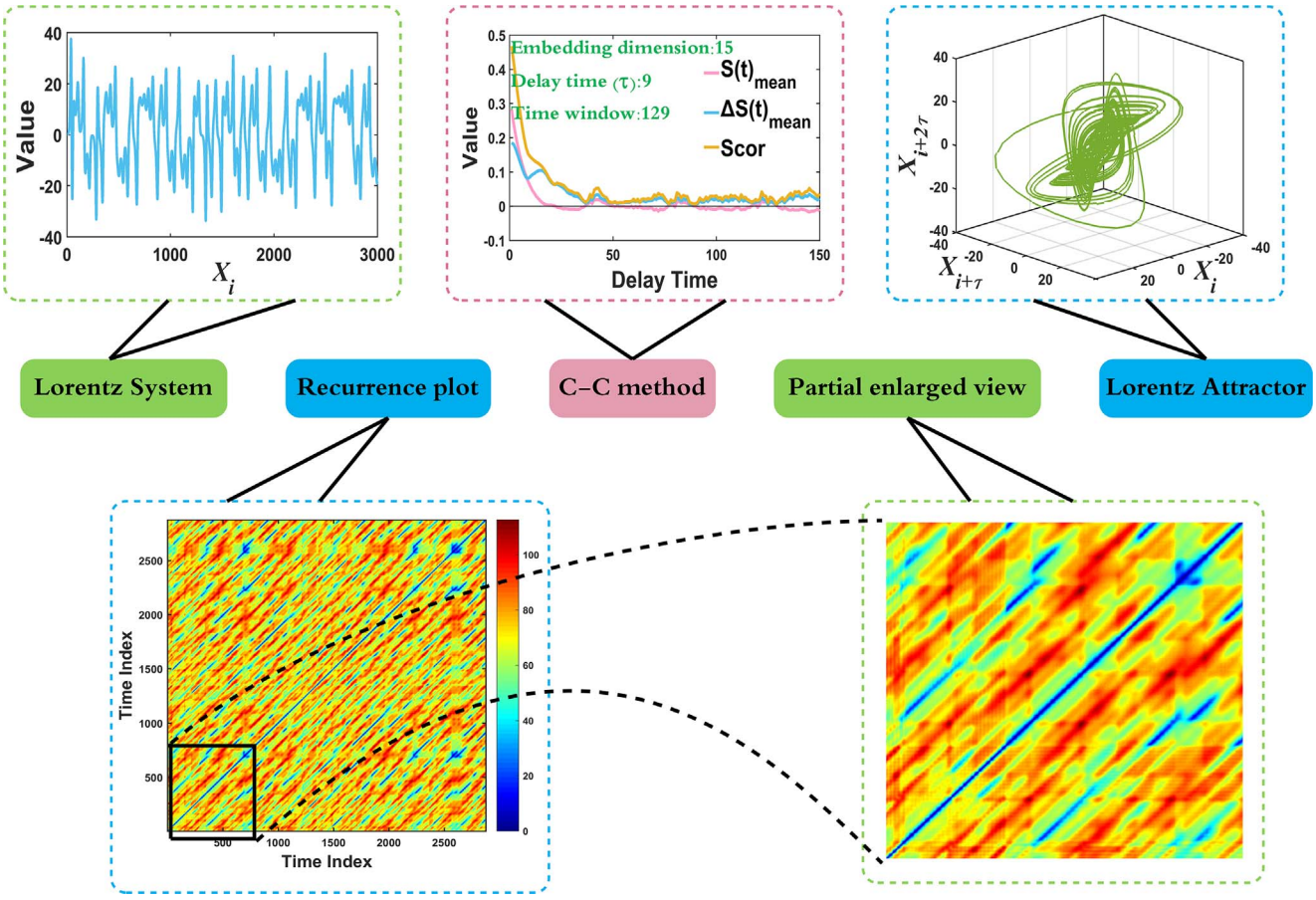

Fig. 1. Illustrative example of recurrence plot.

recurrence plot, which reflects the complexity of the recurrence plot with respect to the diagonal lines.

$$ENTR = -\sum_{l=l_{min}}^{N} p(l)\mathbf{In}p(l) \tag{5}$$

2.2. Feature selection

The effective modeling of complex nonlinear systems has always been a hot topic in the academic community of nonlinear or complex systems. Detection of the immanent mechanism and dynamics is of great significance for modeling a nonlinear system, and this led to the birth of phase space reconstruction. Feature selection through a classical phase space reconstruction technique, namely, the C–C method based on chaos theory, which was proposed by Kim et al. [60], was developed in this study. In the process of phase space reconstruction, accurate determination of the optimal delay time (τ) and embedding dimension (m) is of crucial significance for retrieving the attractor in high-dimensional phase space. Further details of phase space reconstruction based on the C–C method are provided in the following.

Consider a time series $\{x_j | j = 1, 2, \ldots, j\}$. The phase space can be accurately reconstructed in accordance with the aforementioned parameters τ and m, respectively:

$$X_i = [x(i), x(i+\tau), \ldots, x(i+(m-1)\tau)] \tag{6}$$

It is noteworthy that the phase space reconstruction technique provides a new perspective for analyzing the nonlinear system. However, improper, or even inaccurate, determinations of τ and m will lead to significantly negative influences on the effectiveness of the forecast model, such as an unsatisfactory forecast accuracy and potential management risk. The process of phase space reconstruction based on the C–C method comprises the following five steps. More information of the C–C method can be found in Ref. [60].

(1) Determine the suitable length of the time series and then calculate its standard deviation;
(2) Calculate the metrics $S(t)_{mean}$ and $\Delta S(t)_{mean}$.

$$S(t)_{mean} = \frac{1}{16}\sum_{m=2}^{5}\sum_{j=1}^{4} S(m, r_j, \tau) \tag{7}$$

$$\Delta S(t)_{mean} = \frac{1}{4}\sum_{m=2}^{5} S(m,t) \tag{8}$$

where $r_j = j\delta/2$, $j = 1, 2, \ldots, 4$.

(3) Determine the optimal delay time when $S(t)_{mean}$ first reaches zero or first reaches the minimum value.
(4) Coupling the metrics $S(t)_{mean}$ and $\Delta S(t)_{mean}$, the statistic $Scor(t)$ can be obtained when $Scor(t)$ reaches the global minimum, which can be calculated according to:

$$Scor(t) = \Delta S(t)_{mean} + |S(t)_{mean}| \tag{9}$$

(5) The optimal time window ϖ can be determined when $Scor(t)$ reaches the global minimum value. Furthermore, the m can be obtained via the Eq. (10).

$$\varpi = (m-1)\tau \tag{10}$$

2.3. Multi-input multi-output least squares support vector machine

In this section, a classical machine learning model MIMOLSSVM, which is applied to perform the interval prediction, is introduced. In addition, the proposed IMOWCA to further optimize the performance of MIMOLSSVM is described.

The MIMOLSSVM model, based on the principle of structural risk minimization [61–63], is a powerful tool for implementing interval prediction via the multi-output pattern. However, the application of MIMOLSSVM to uncertainty modeling is rarely implemented, despite the fact that it has excellent nonlinear system modeling capabilities, in particular for uncertainty mining.

Consider the training dataset as $\boldsymbol{T} = x_i, y_i^n$, where x_i belongs to $\mathscr{R}^p$, y_i belongs to $\mathscr{R}^d$, and x_i and y_i represent the input and output dataset of the training set, respectively. Additionally, $\mathscr{R}^p$ denotes the input space with the dimension of p; the dimension p is optimally and dynamically determined according to the obtained embedding dimension via the aforementioned C−C method, and $\mathscr{R}^d$ is selected as the value of 2 considering the prediction interval with the upper and lower bound in this study. Technically, the classical LSSVM can be formulated as:

$$y = w^T\boldsymbol{\phi}(x) + b \tag{11}$$

where w and b denote the weights and the bias, respectively, and $\boldsymbol{\phi}$ signifies the function mapping stemming from the nonlinear relationship between input and output sets. More details of LSSVM can be found in Ref. [64].

The classical LSSVM model has an excellent ability to model the nonlinear series with the pattern of single-output. However, the LSSVM model with single output does not evidently meet the requirement that interval prediction be implemented, leading to inferior forecast results, even if two or more single LSSVM models are combined into a multi-output LSSVM, because this overlooks the combined fitting bias generated by multiple LSSVM models. Accordingly, MIMOLSSVM was developed in this study to perform the interval prediction. The detailed theory of MIMOLSSVM can be found in Ref. [65].

2.4. Introduction to the improved multi-objective water cycle algorithm

In this section, the flow of the original water cycle algorithm (WCA) is introduced. Furthermore, the improved multi-objective water cycle algorithm (IMOWCA), aimed at optimizing the devised forecast module, is proposed. It is described as follows.

2.4.1. Water cycle algorithm

Inspired by the actual water cycle process, the single-objective WCA, which is extensively applied in many fields, such as electrical power system [66,67] and traffic light scheduling [68], was proposed by Eskandar et al. [69]. The calculation process of the WCA is as follows. The initial population of size N_{pop} can be obtained randomly. It is divided into two sections in accordance with the fitness values. The first section consists of N_{sr} raindrops, which have a better fitness than the second section. The best raindrop and some rivers are grouped in the first section. The second section is composed of many raindrops, which are called the streams in this algorithm. The size of the streams, which are allocated to the aforementioned first section, can be calculated according to Eq. (12), where $\boldsymbol{Cost}_n$ represents the fitness value of the n-th raindrop.

$$NS_n = \mathbf{round}\left\{\left|\frac{\boldsymbol{Cost}_n}{\sum_{k=1}^{N_{sr}}\boldsymbol{Cost}_k}\right| \times (N_{pop}-N_{sr})\right\}, n = 1,2,...,N_{sr} \tag{12}$$

Further, the algorithm consists of the following steps.

Step 1: The iterative process of the new positions of streams and rivers ($\vec{\mathbf{X}}_{Stream}^{i+1}, \vec{\mathbf{X}}_{River}^{i+1}$) can be expressed as Eqs. (13)–(15), which describe how the streams and rivers move toward sea while updating their positions. It is noteworthy that the optimum determination of C is 2, which was proposed in [66]; **rand** is a value that obeys the uniform random distribution in the range [0,1].

$$\vec{\mathbf{X}}_{Stream}^{i+1} = \vec{\mathbf{X}}_{Stream}^{i} + \mathbf{rand} \times C \times (\vec{\mathbf{X}}_{River}^{i} - \vec{\mathbf{X}}_{Stream}^{i}) \tag{13}$$

$$\vec{\mathbf{X}}_{Stream}^{i+1} = \vec{\mathbf{X}}_{Stream}^{i} + \mathbf{rand} \times C \times (\vec{\mathbf{X}}_{Sea}^{i} - \vec{\mathbf{X}}_{Stream}^{i}) \tag{14}$$

$$\vec{\mathbf{X}}_{River}^{i+1} = \vec{\mathbf{X}}_{River}^{i} + \mathbf{rand} \times C \times (\vec{\mathbf{X}}_{Sea}^{i} - \vec{\mathbf{X}}_{River}^{i}) \tag{15}$$

Step 2: The positions of each river and stream are automatically exchanged when the fitness of the stream is better than that of the rivers. Similarly, the position of the sea is replaced with its assigned stream or river when their fitness value is greater than that of the sea.

Step 3: The behavior of evaporation and precipitation is triggered on condition that the evaporation condition, as shown in Eq. (16), is satisfied. Consequently, the position of streams is initialized, leading to the new positions of streams according to Eq. (17). Furthermore, the optimal position of a stream is considered to be the river that flows toward the sea. Analogically, the new position of the stream can be calculated according to the stream that flows to the sea if the evaporation condition is satisfied, shown in Eq. (18). The noteworthy point is that the operation of evaporation can reduce the probability that the algorithm falls prematurely into local optima.

$$|\vec{\mathbf{X}}_{Sea}^{i} - \vec{\mathbf{X}}_{\kappa}^{i}| < d_{max}^{i}, \kappa \in \{Stream, River\} \tag{16}$$

$$\vec{\mathbf{X}}_{New\ Stream}^{i} = \mathbf{LB} + \mathbf{rand} \times (\mathbf{UB} - \mathbf{LB}) \tag{17}$$

$$\vec{\mathbf{X}}_{New\ stream}^{i} = \vec{\mathbf{X}}_{Sea}^{i} + \sqrt{\mu} \times \mathbf{Randn} \tag{18}$$

where d_{max} is set as 10^{-6}, and **Randn** is a random vector that obeys uniform distribution with the range $[-1,1]$. Additionally, **LB** and **UB** represent the lower and upper bounds of variables. Finally, μ was set as 0.1 in the study [66].

Step 4: The tolerance in the evaporation condition, namely d_{max}, adaptively decreases in the process of iteration, which is shown in

$$d_{max}^{i+1} = d_{max}^{i} - \frac{d_{max}^{i}}{maxiteration} \tag{19}$$

Step 5: The algorithm is finalized if the end condition (such as maximum iteration numbers) is satisfied; Otherwise, it returns to **Step 1**.

2.4.2. Improved multi-objective water cycle algorithm

The innovation of the IMOWCA proposed in this paper is that the adaptive and nonlinear inertia weight (ω), which has an excellent capability to balance the global and local search capability in the process of algorithm iterations, as shown in Eq. (20), is introduced into the original MOWCA for the first time. Technically, when ω is large, the IMOWCA has an excellent global exploration capability, while its local exploitation ability is poor; conversely, the IMOWCA has noteworthy superiority in terms of local exploitation, while its global exploration ability is poor. Accordingly, determining the appropriate ω can balance the capability of global exploration and local exploitation in IMOWCA, which can significantly promote the convergence rate and effectiveness of MOWCA. The improved iteration formulations on the new position of streams and rivers in IMOWCA can be formulated as in Eq. (21). Additionally, as well as the detailed calculation process of the MOWCA, the reports in [66,70,71] provide large amounts of information about this algorithm.

$$\begin{cases}\omega_j = \omega_{end} + (\omega_{start} - \omega_{end}) \times \mathbf{exp}(-3.5 \times (j/maxiteration))^3 \\ j = 1,2,...,maxiteration\end{cases} \tag{20}$$

$$\begin{cases} \vec{\mathbf{X}}_{Stream}^{i+1} = \vec{\mathbf{X}}_{Stream}^{i+1} + \omega_j \times \mathbf{rand} \times C \times (\vec{\mathbf{X}}_{River}^{i} - \vec{\mathbf{X}}_{Stream}^{i}) \\ \vec{\mathbf{X}}_{Stream}^{i+1} = \vec{\mathbf{X}}_{Stream}^{i} + \omega_j \times \mathbf{rand} \times C \times (\vec{\mathbf{X}}_{Sea}^{i} - \vec{\mathbf{X}}_{Stream}^{i}) \\ \vec{\mathbf{X}}_{River}^{i+1} = \vec{\mathbf{X}}_{River}^{i} + \omega_j \times \mathbf{rand} \times C \times (\vec{\mathbf{X}}_{Sea}^{i} - \vec{\mathbf{X}}_{River}^{i}) \end{cases} \quad (21)$$

The complexity of IMOWCA is as follows. The complexity of IMOWCA is $O(N_{pop}^2)$ in the worst scenario. The detailed computation processes are as shown in Table 3, where M denotes the number of objective functions and N_{pop} represents the population size in IMOWCA.

In order to compare the proposed IMOWCA with other multi-objective optimization algorithms, a literature review on the subject of the complexity measurement of multi-objective optimization algorithms was conducted. The complexity of the considered multi-objective optimization algorithms is as follows. The complexity of NSGA-II [73], SPEA2 [74] and PAES [75] is $O(MN_{pop}^2)$ and the complexity of NSGA [76] and SPEA [77] is $O(MN_{pop}^3)$. Obviously, the IMOWCA has a lower complexity than these algorithms, which indicates that its computational efficiency is high as compared to that of these benchmark algorithms.

Importantly, the IMOWCA was developed in this study to dynamically optimize the parameter configuration in the forecast module, with the aim of improving the efficiency and effectiveness of the devised forecast module.

2.4.3. Testing of improved multi-objective water cycle algorithm

In order to validate the effectiveness and efficiency of IMOWCA as compared to MOWCA, the four testing problems described in Appendix A were performed on the platform of **MATLAB** R2015b on Microsoft Windows 7 with 3.30 GHz Intel Core i5-4590 HQ 64-bit and 8 GB of RAM. The algorithm parameters of IMOWCA and MOWCA are displayed in Table 4. Additionally, in order to obtain robust and effective simulation results, each algorithm was repeatedly simulated 20 times, and then, the final results were obtained by averaging the obtained results. Generational distance (GD) [78,79] and spacing (SP) [80,81] were applied to quantitatively evaluate the performance of the two algorithms. The GD, proposed in [78], is used to measure the distance between the true Pareto front and obtained Pareto front. Accordingly, the smaller the value of GD, the better the performance of the multi-objective algorithm. The SP is usually applied to evaluate the distributivity of solutions in a Pareto set. All non-dominant solutions are equidistant (or even) if the SP is equal to 0. In Table 5, the final simulation results are displayed, from which it can be concluded that IMOWCA is significantly superior to the original MOWCA on balance. The efficiency of IMOWCA is slightly superior to that of original MOWCA in the problems of ZDT1, ZDT3, and Kursawe, according to the computation times shown in Table 5. In order to further illustrate the comparative performance of IMOWCA and MOWCA, the corresponding Pareto fronts obtained by IMOWCA and MOWCA are visualized in Fig. 2, in which it can be observed that the Pareto front obtained by IMOWCA is closer to the true Pareto front than that obtained by MOWCA.

3. System development

In this section, the overall frame structure of the devised analysis-forecast system is systematically described, as well as the three popular metrics used for evaluating the performance of uncertainty modeling.

3.1. System design

As shown in Fig. 3, the overall framework of the devised analysis-forecast system is composed of the following steps.

(1) In order to reduce the complexity generated by the raw wind speed series, an effective frequency-time analysis based on the CEEMDAN method was developed to decompose the wind speed series into mode components.
(2) To analyze and explore the nonlinear dynamical mechanism of wind speed series and the corresponding IMFs, recurrence analysis techniques based on chaos theory were developed to perform the qualitative and quantitative investigation for wind speed series.
(3) To ensure the efficiency of the devised system, the IMFs generated from the original wind speed series are effectively merged according to the corresponding complexity degree.
(4) The C–C method based on chaos theory was developed to determine the optimal input forms of the forecast module according to the obtained delay time and embedding dimension, which improves the efficiency of the reconstruction of the model input.
(5) Furthermore, the input and output forms of the forecast module can be expressed as Eqs. (22) and (23), where $\boldsymbol{\alpha}$ denotes the interval width coefficient, and parameters τ and m represent the delay time and embedding dimension, respectively.

$$\textbf{\textit{Input set}}: \begin{bmatrix} x_1 & x_{n-(m-1)\tau} \\ x_{1+\tau} & x_{n-(m-2)\tau} \\ x_{2+\tau} & x_{n-(m-2)\tau} \\ \vdots & \vdots \\ x_{1+(m-1)\tau} & x_{n-1} \end{bmatrix} \quad (22)$$

$$\textbf{\textit{Output set}}: \begin{bmatrix} x_{1+(m-2)\tau} \times (1-\boldsymbol{\alpha}) & x_{1+(m-2)\tau} \times (1+\boldsymbol{\alpha}) \\ x_{2+(m-2)\tau} \times (1-\boldsymbol{\alpha}) & x_{2+(m-2)\tau} \times (1+\boldsymbol{\alpha}) \\ x_{3+(m-2)\tau} \times (1-\boldsymbol{\alpha}) & x_{3+(m-2)\tau} \times (1+\boldsymbol{\alpha}) \\ \vdots & \vdots \\ x_n \times (1-\boldsymbol{\alpha}) & x_n \times (1+\boldsymbol{\alpha}) \end{bmatrix} \quad (23)$$

(6) More importantly, the IMOWCA proposed in this study was effectively developed to optimize the key parameters of MIMOLSSVM in the devised forecast module.
(7) Finally, the final prediction intervals can be obtained via merging the forecasting results generated by each IMF.

3.2. System evaluation

In order to quantitatively assess the effectiveness of the devised forecast module, the metrics coverage probability (*CP*) and average width (*AW*) were applied in the evaluation module. Moreover, the accumulated width deviation (*AWD*) metric was also used to assess the reliability of the forecast module.

The accuracy of prediction intervals can be obtained by the *CP* metric, which reflects the probability that the actual observed value z_i falls within the constructed prediction interval. *CP* can be calculated by

$$CP = \frac{1}{n}\sum_{i=1}^{n} c_i, c_i = \begin{cases} 1 \; z_i \in [\boldsymbol{L}_i, \boldsymbol{U}_i] \\ 0 \; z_i \notin [\boldsymbol{L}_i, \boldsymbol{U}_i] \end{cases} \quad (24)$$

where c_i signifies a Boolean value and $\boldsymbol{L}_i$ and $\boldsymbol{U}_i$ denote the lower and

Table 3
Complexity analysis of improved multi-objective water cycle algorithm.

Algorithm procedures	Complexity
Determination of the sea	$O(N_{pop}^2)$ [72]
Move streams and rivers	$O(N_{pop})$ [72]
Replace rivers and sea by better streams and rivers, respectively	$O(N_{pop})$ [72]
Check the evaporation condition	$O(N_{pop})$ [72]
Non-dominated sorting	$O(M(3N_{pop})^2)$ [73]
Crowding distance assignment	$O(M(3N_{pop})\log(3N_{pop}))$ [73]
Rank-crowd sorting procedure	$O(M(3N_{pop})\log(3N_{pop}))$ [73]

Table 4
Parameter settings of the improved multi-objective water cycle algorithm and the multi-objective water cycle algorithm.

Parameter configuration	IMOWCA	MOWCA
Population size	200	200
Size of archive	100	100
Maximum iteration	200	200
Number of streams	196	196
Number of rivers and seas	4	4
Evaporation condition constant	1×10^{-2}	1×10^{-6}
Initial value of inertia weight ω_{start}	0.9	–
Terminal value of inertia weight ω_{end}	0.4	–

upper bound of the constructed prediction interval, respectively. Parameter n represents the number of prediction intervals.

Given the appropriate CP, the smaller the AW value, the better is the system performance is. The metric AW can be calculated by

$$AW = \frac{1}{n}\sum_{i=1}^{n}(\boldsymbol{U}_i - \boldsymbol{L}_i) \tag{25}$$

AWD can be calculated by measuring the relative deviation degree, which can be obtained by the cumulative sum of AWD_i. The calculation formula of AWD is expressed as Eqs. (26) and (27), where $\boldsymbol{\alpha}$ denotes the interval width coefficient and $\boldsymbol{I}_i$ represents the i-th prediction interval.

$$AWD_i = \begin{cases} \dfrac{\boldsymbol{L}_i^{(\alpha)} - z_i}{\boldsymbol{U}_i^{(\alpha)} - \boldsymbol{L}_i^{(\alpha)}}, & z_i < \boldsymbol{L}_i^{(\alpha)} \\ 0, & z_i \in \boldsymbol{I}_i^{(\alpha)} \\ \dfrac{z_i - \boldsymbol{U}_i^{(\alpha)}}{\boldsymbol{U}_i^{(\alpha)} - \boldsymbol{L}_i^{(\alpha)}}, & z_i > \boldsymbol{U}_i^{(\alpha)} \end{cases} \tag{26}$$

$$AWD^{(\alpha)} = \frac{1}{n}\sum_{i=1}^{n} AWD_i^{(\alpha)} \tag{27}$$

Importantly, it is worth mentioning that the metrics $-CP$ and AW were determined as the objective functions of IMOWCA in this study.

4. Numerical simulations and results analysis

In this section, the sites included in this study and the data are described. Furthermore, certain statistical metrics are used to express the basic characteristics of wind speed series. In this study, recurrence analysis techniques were effectively developed to study the dynamic characteristics in phase space and uncover the rhythmicity of the nonlinear dynamics system based on wind speed series. Finally, uncertainty modeling, which was effectively performed based on wind speed series from two wind farms, is described.

4.1. Study sites and data source

In this section, wind speed series from two wind farms, namely, the Penglai site (37.48°N, 120.45°E) and Chengde site (40.97°N, 117.93°E) in China, were selected as the experimental data to verify the devised analysis-forecast system. As shown in Table 6, five statistical indexes Min, Max, Std. (standard deviation), complexity and maximum Lyapunov exponent (MLYE) based on the wolf method [82], were used to perform the descriptive statistical analysis of the data used in this study. Theoretically, the studied nonlinear system can be assumed to be a chaotic dynamic system if the maximum Lyapunov exponent is greater than zero. In particular, it is noteworthy that the MLYEs of the data in Table 6 are all greater than zero, which indicates that the wind speed series in this study are essentially chaotic time series. The basic information of the sites and the raw wind speed data, including the training and testing sets, are displayed in Fig. 4.

4.2. Implementing uncertainty analysis and modeling

In this section, we describe how uncertainty modeling is effectively performed based on the nonlinear system of wind speed from two wind farms in China. Frequency domain decomposition based on the CEEMDAN technique is effectively applied to wind speed series. Then, the use of feature selection based on the C–C method to dynamically select the most qualified input forms is described. In addition, the development of the recurrence analysis techniques to explore the dynamic properties of wind speed series is presented. Finally, the effective simulation of the devised system to test its robustness and effectiveness is described.

4.2.1. Frequency domain decomposition

Because of the complex non-linearity of wind speed series, frequency domain decomposition for wind speed series is vital. CEEMDAN was developed in this study to implement our method. It is noteworthy that no single theory can be used to effectively determine the number of IMFs far. In this study, the determination of the number of IMFs depended mainly on empirical study. The detailed parameters of CEEMDAN were as follows: the number of IMFs was 12; the standard deviation of the added Gaussian white noise was 0.2; the number of realizations was 500; and the maximum number of sifting iterations allowed was 5000. In order to reduce the modeling complexity and enhance the efficiency of the devised system, the IMFs (IMF1–IMF12) generated by the CEEMDAN method were merged as shown in Fig. 5, according to the corresponding complexity of each IMF, obtaining reconstructed IMFs (IMF1–IMF7). The complexity degree and MLYE of these reconstructed IMFs are displayed in Table 7. In Particular, it can be confirmed substantially that these reconstructed IMFs are chaotic time series according to the MLYE in Table 7, which are all greater than 0.

Table 5
Assessment results of improved multi-objective water cycle algorithm and the multi-objective water cycle algorithm.

Problem	Algorithm	CPU time (s)	GD					SP				
			Best	Average	Median	Worst	Std.	Best	Average	Median	Worst	Std.
ZDT1	IMOWCA	29.7280	0.0015	**0.0039**	0.0030	**0.0124**	**0.0026**	**0.0619**	0.0796	0.0801	**0.0933**	**0.0081**
	MOWCA	29.8663	**0.0013**	0.0094	0.0030	0.0896	0.0189	0.0151	**0.0740**	**0.0769**	0.0979	0.0169
ZDT3	IMOWCA	29.4013	**0.0049**	**0.0064**	**0.0062**	**0.0085**	**0.0014**	0.1705	0.2066	0.2034	0.2808	**0.0447**
	MOWCA	30.6576	0.0053	0.0167	0.0135	0.0641	0.0138	**0.0651**	**0.1712**	**0.1756**	**0.2585**	0.0540
Kursawe	IMOWCA	30.9350	**0.0953**	**0.1146**	**0.1220**	**0.1265**	**0.0169**	1.1172	**1.2180**	**1.2587**	**1.2783**	**0.0879**
	MOWCA	34.8924	0.1359	0.1661	0.1536	0.1981	0.0291	**0.8565**	1.7162	1.5509	2.4648	0.6533
Viennet3	IMOWCA	31.8706	**0.0038**	**0.0057**	**0.0048**	**0.0082**	**0.0021**	2.2716	2.5119	2.5766	**2.7831**	0.2106
	MOWCA	30.6787	0.0046	0.0129	0.0114	0.0313	0.0064	**2.0812**	**2.4289**	**2.4157**	2.9181	**0.2048**

Bold characters: the best results among all the algorithms.

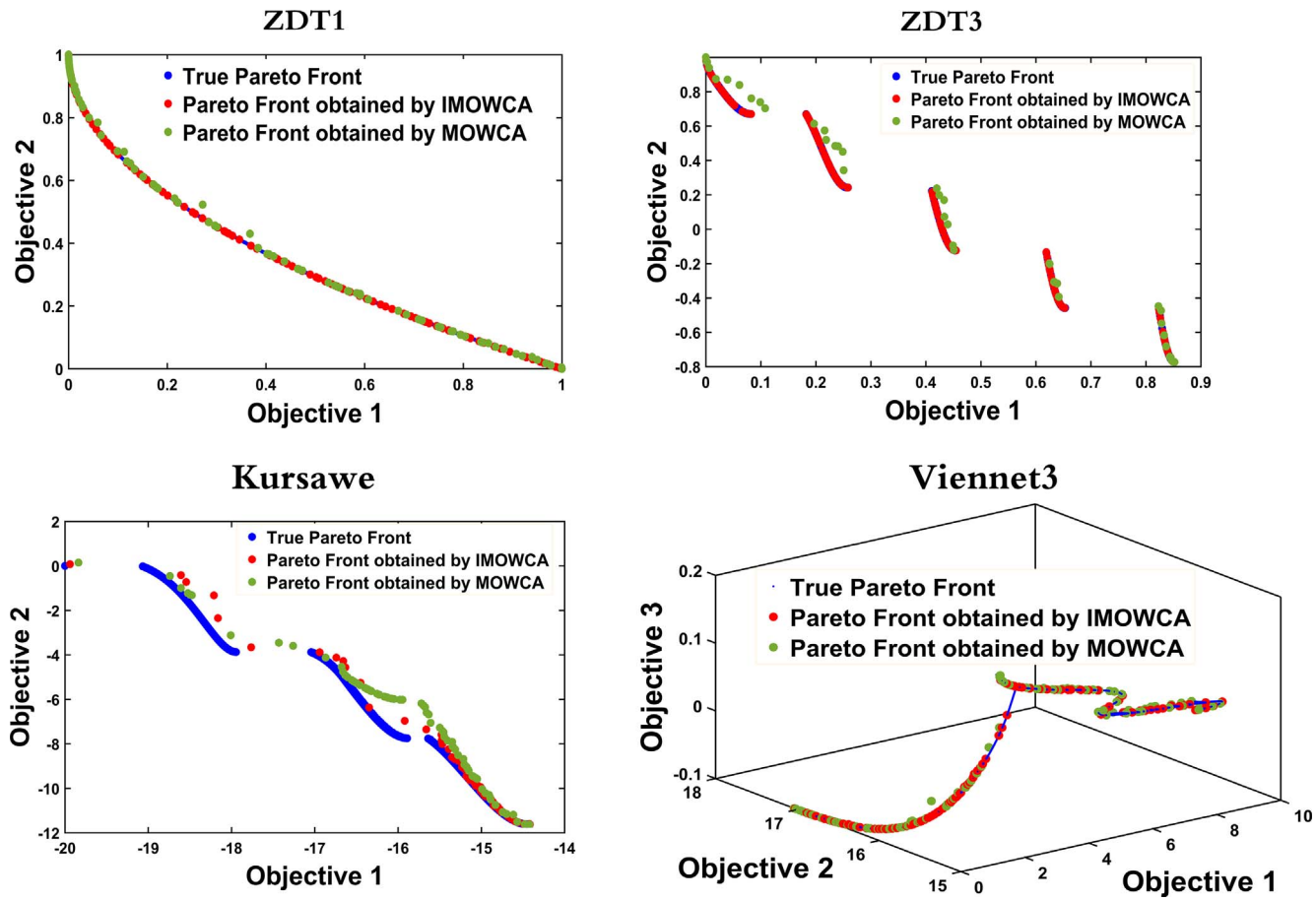

Fig. 2. Obtained Pareto fronts of improved multi-objective water cycle algorithm and the multi-objective water cycle algorithm.

4.2.2. Feature selection based on phase space reconstruction

The determination of the suitable input forms for the devised system plays a vital role in the process of uncertainty modeling. Inversely, inapposite input forms will exert a significantly negative impact on the forecast accuracy and effectiveness. Accordingly, the C−C method based on chaos theory was developed to dynamically determine the optimal input forms. Technically, the merits of the feature selection based on the C−C method are as follows: (1) model simplification [83]; (2) model efficiency enhancement; (3) avoidance of the curse of dimensionality; and (4) model generalization enhancement by reducing over-fitting [84]. The C−C method parameters of the wind speed series and corresponding IMFs are presented in Table 8. In order to effectively exhibit the attractor and its trajectories of wind speed series, the attractor of each IMF based on wind speed data from Penglai site 1 was retrieved, according to the corresponding delay time obtained by using the C−C method, as shown in Fig. 6. It can be seen in this figure that the attractor is clearer and more unfolded from IMF1 to IMF7. The aforementioned analysis indicates that the predictability of IMF increases from IMF1 to IMF7.

4.2.3. Uncertainty analysis

The investigation and analysis of the dynamic characteristics and predictability in advance has an important significance for uncertainty modeling. In order to qualitatively perform the analysis for the wind speed series, the original wind speed series and the corresponding IMF were transformed into recurrence plots according to the corresponding delay time and embedding dimension. Furthermore, the recurrence quantification analysis including certain metrics was used to quantitatively analyze and study the dynamic characteristics of the complex nonlinear system based on wind speed data.

In order to effectively reconstruct the phase space, it is crucial to acquire the optimal delay time and embedding dimension. According to the delay times and embedding dimensions in Table 8, the original wind speed series and the corresponding IMFs could be transformed into recurrence plots, which are visualized in Fig. 7. Fig. 7(A) –(C) show the data from Penglai site 1, Penglai site 2, and Chengde site 1, respectively.

Fig.7 indicates the following:

(1) In the recurrence plot of Penglai site 1 shown in Fig. 7(A), there are some short navy-blue diagonal lines, which simultaneously occur beside some single isolated points. The figure also further indicates that the wind speed series is chaotic. Additionally, the red bands signify that there is nonstationarity (or a drastic change). In Fig. 7(A), a roughly homogeneous phenomenon appears in the recurrence plots of IMF1–IMF4, which shows that a large number of single isolated points occur in these figures. The appearance of plentiful single isolated points and frequent red bands significantly illustrates that the series IMF1–IMF4 is extremely unstable, exposing the randomness and high volatility of wind speed series. The recurrence plots from IMF5 and IMF6 start to show some diagonal lines, which illustrates that the evolution of states in phase space is comparable at different times. There are some longer diagonal lines in the recurrence plots of IMF6 and IMF7, which indicates that the level of predictability is increasing gradually.

(2) It can be seen in the texture of the recurrence plot based on Penglai site 2 in Fig. 7(B) that a homogeneous structure sometimes similarly occurs in the navy-blue squared block, which signifies that the stationary process is embedded into the nonlinear system based on wind speed series. Additionally, vertical recurrence points occur within the blocks, which indicates that it is a chaos system among laminar zones. Similarly, there is an approximately homogeneous

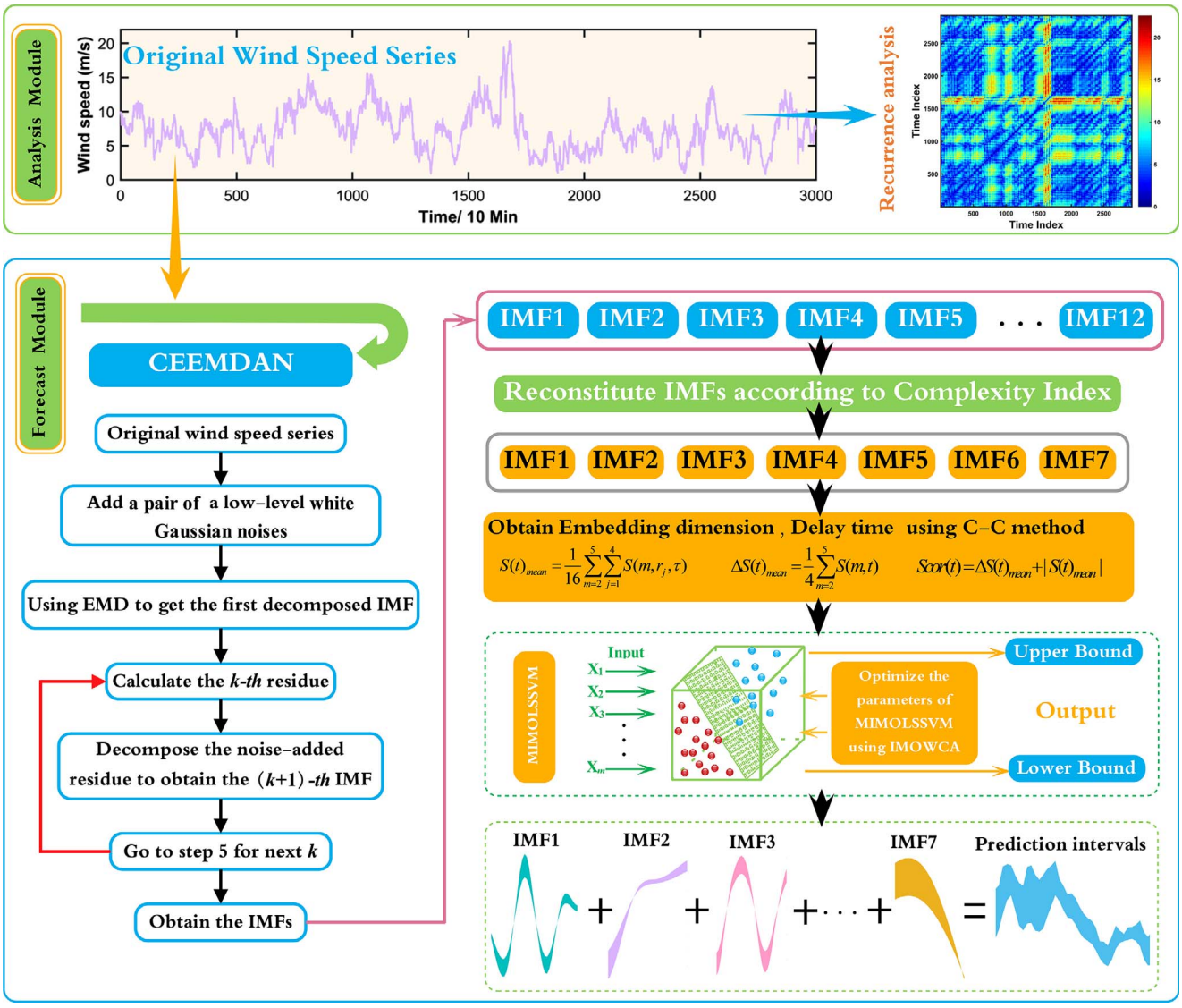

Fig. 3. Overall framework of the devised analysis-forecast system.

Table 6
Statistical descriptions of the data.

Sites	Data	Number	Min (m/s)	Max (m/s)	Std. (m/s)	Complexity	MLYE
Penglai site 1	All samples	3000	0.8	20.3	3.1379	0.3933	0.2432
	Training set	2600	0.9	20.3	3.1994	0.3988	0.2555
	Testing set	400	0.8	13.1	2.6134	0.4340	0.1525
Penglai site 2	All samples	3000	0.9	18.5	3.6152	0.3953	0.1592
	Training set	2600	0.9	18.5	3.6791	0.4012	0.1534
	Testing set	400	1.1	17.1	2.6444	0.5666	0.0417
Chengde site 1	All samples	3000	0.2	20.6	3.3785	0.5104	0.1818
	Training set	2600	0.2	20.5	3.2912	0.4961	0.1564
	Testing set	400	1.6	20.6	3.4708	0.6751	0.1972

texture among the recurrence plots of IMF1–IMF3, displaying many navy-blue points with a uniform form, which further illustrates that the original wind speed data contain intrinsic random components. However, the navy-blue diagonal lines first appear in the recurrence plot of IMF4. Furthermore, there are longer diagonal lines in IMF6 and IMF7, in particular in IMF7. Additionally, some red clusters with vertical and horizontal texture appear, where an abrupt transition or change occurs.

(3) In Fig. 7(C), the wind speed series and the corresponding IMFs from Chengde site 1 were converted into recurrence plots according to the corresponding delay time and embedding dimension. In the recurrence plot based on the wind speed series from Chengde site 1, there are very few navy-blue diagonal lines, which indicates there is strong indeterminacy and randomness in the wind speed data of this site. The indeterminacy and randomness makes uncertainty modeling challenging. As similar to Fig. 7(A) and (B), IMF1–IMF3 also exhibit a similar texture with many navy-blue points, which means that these frequency domains have strong randomness

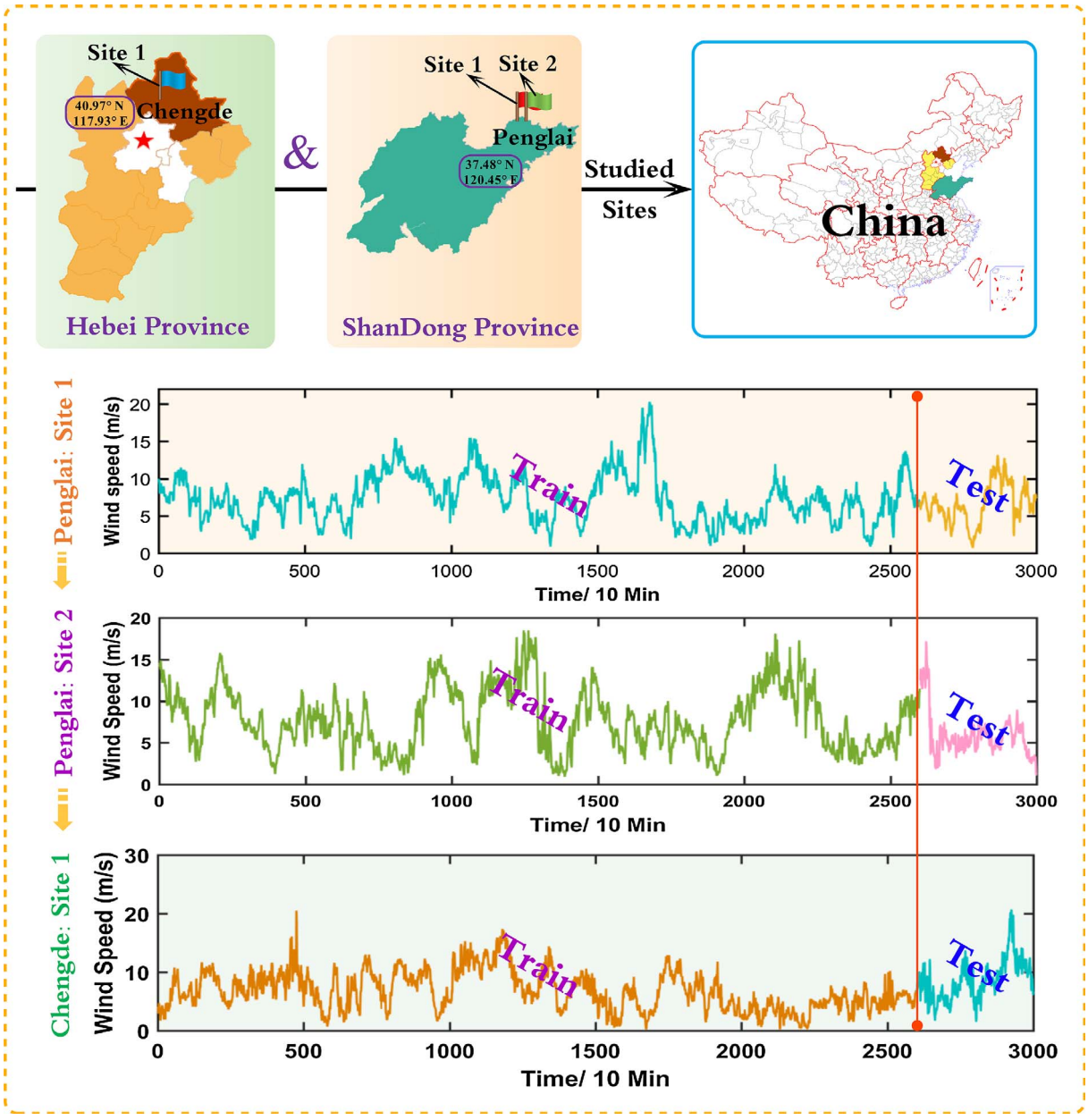

Fig. 4. Sites and data.

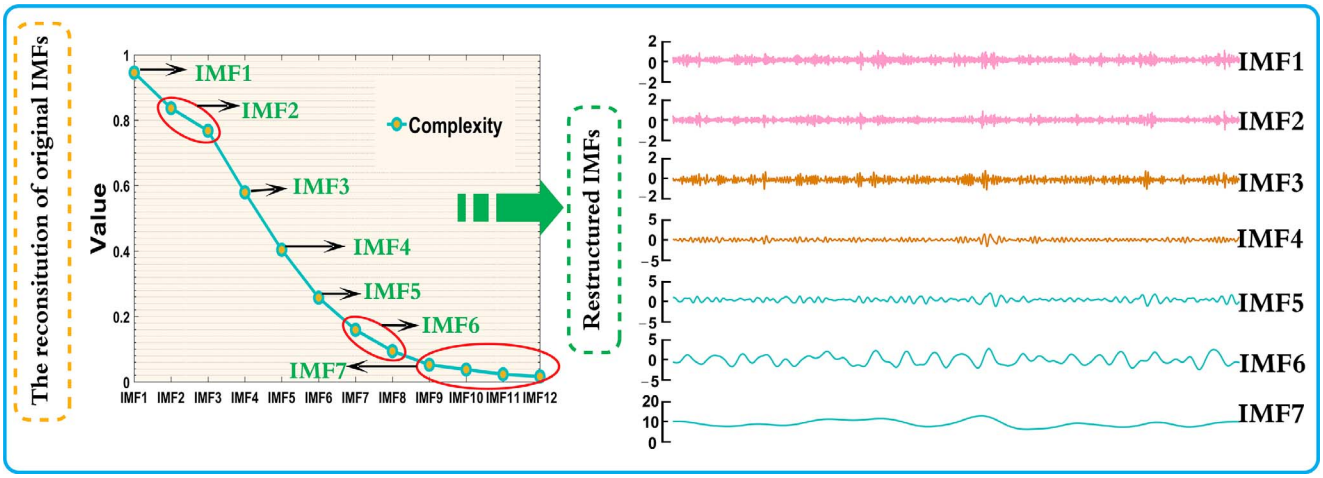

Fig. 5. Results of reconstructed intrinsic mode functions based on Penglai Site 1.

Table 7
Complexity degree and of maximum Lyapunov exponent each intrinsic mode function.

Sites	Indexes	IMF1	IMF2	IMF3	IMF4	IMF5	IMF6	IMF7
Penglai site 1	Complexity	0.9455	0.7865	0.5794	0.4037	0.2573	0.1381	0.0397
	MLYE	0.4457	0.0149	0.0573	0.0167	0.0079	0.0122	0.0054
Penglai site 2	Complexity	0.9350	0.7593	0.5878	0.4225	0.2677	0.1130	0.0523
	MLYE	0.2874	0.0054	0.0102	0.0227	0.0347	0.0029	0.0066
Chengde site1	Complexity	0.9141	0.7698	0.5962	0.4267	0.2740	0.1422	0.0439
	MLYE	0.1167	0.0051	0.0068	0.0460	0.0050	0.0092	0.0147

Table 8
Parameters m, τ, and ϖ generated by the C−C method.

Indexes	Penglai site 1	IMF1	IMF2	IMF3	IMF4	IMF5	IMF6	IMF7
m	3	5	17	6	10	8	4	5
τ	37	10	2	4	8	16	31	33
ϖ	69	44	32	20	72	115	101	121
Indexes	Penglai site2	IMF1	IMF2	IMF3	IMF4	IMF5	IMF6	IMF7
m	4	7	26	12	8	4	7	8
τ	33	7	2	4	8	16	25	18
ϖ	93	45	50	45	55	53	141	121
Indexes	Chengde site1	IMF1	IMF2	IMF3	IMF4	IMF5	IMF6	IMF7
m	5	9	48	19	6	10	5	7
τ	30	5	2	4	8	15	31	21
ϖ	117	40	93	71	36	133	122	128

components. Moreover, there are some periodic recurrent structures (the longer diagonal lines, checkerboard structures) in the recurrence plots of IMF4–IMF7, which indicates that the predictability of frequency domains is increasing gradually.

However, it is not sufficient to rely merely on subjective observation to investigate recurrence plots. Accordingly, in this study, evaluation metrics of the recurrence plots were used to quantitatively evaluate them.

Recurrence quantification analysis is an effective technique to investigate the phenomena of transitions, mutation, and periodicity in the system dynamics in time series. Table 9 shows some quantitative results of the aforementioned recurrence plots, which indicate the following.

(1) A higher *RR*, *DET*, and *L* represent higher predictability. As compared to the wind speed data from Penglai sites 1–2, the predictability of the data from the Chengde farm is lower according to the metrics considered in this study. Additionally, the *ENTR* of wind speed data from Penglai site 2 is higher than from Penglai site 1 and Chengde site 1, which illustrates that the complexity of the recurrence plot based on the data from Penglai site 2 is higher than that for other sites.
(2) In all cases, in addition to the high frequency domains, namely, IMF1–IMF3, the four metrics increase from IMF4–IMF7, which significantly illustrates that IMF4–IMF7 generated by CEEMDAN are the main frequency domains of the studied wind speed series. However, merely modeling the main frequency does not suffice to quantify the uncertainty. Accordingly, in this study, each IMF, including the high frequency domain and main frequency domain, was effectively modeled to further mine the uncertainty in wind speed series.

Remark. Given the evaluation metrics in Table 9, the wind speed series from Chengde site 1 has lower predictability because its *RR*, *DET*, and *L* are lower than those of Penglai sites 1–2. Accordingly, to effectively perform uncertainty mining for Chengde site 1 is a challenging task.

4.2.4. Uncertainty mining

In this section, three cases based on wind speed series from two different wind farms in China are used to validate the effectiveness and robustness of the devised forecast module aimed at quantifying uncertainties. Three benchmark models, Modes-MOWCA-CC-MIMOLSSVM, IMOWCA-CC-MIMOLSSVM, and IMOWCA-MIMOLSSVM, were used in this study in order to reveal the superiority of the devised system. Importantly, the crucial parameters of the forecast module were dynamically tuned by IMOWCA in order to ensure the robustness and accuracy of the system. The detailed parameter settings of IMOWCA are displayed in Table 10. Additionally, three statistical metrics, namely, *CP*, *AW*, and *AWD*, were applied to further evaluate the accuracy and appropriateness of the devised forecast module.

The quantitative simulation results of interval prediction are shown as in Tables 11 and 12, which consist of the simulations based on Penglai site 1, Penglai site 2, and Chengde site 1, respectively. All the numerical simulations were conducted on the platform of **MATLAB** R2015b on Microsoft Windows 7 with 3.30 GHz Intel Core i5-4590HQ 64-bit and 8 GB of RAM. All the cases in this study were effectively implemented based on interval width coefficients 0.1 and 0.2. To consider the randomness in the process of the simulations, the obtained results shown in Tables 11 and 12 were determined via averaging the results of 10 experiments. Technically, the assessment of interval prediction is usually related to *CP* and *AW*. However, there is a contradictory relationship between *CP* and *AW*. Clearly, *CP* increases when *AW* increases, which reduces the informativeness of prediction intervals and increases risk. Accordingly, *AWD* was introduced to effectively evaluate the accuracy of prediction intervals. Additionally, in order to illustrate the detailed prediction intervals of all the cases, Figs. 8–10 exhibit the performance of the devised forecast module and the benchmark models that were considered, respectively.

In order to further investigate the experimental results, Tables 11 and 12 and Figs. 8 and 10 reveal the following.

(1) A comparison of Modes-IMOWCA-CC-MIMOLSSVM and Modes-MOWCA-CC-MIMOLSSVM reveals that, in all cases, the devised forecast module is notably superior to all the benchmark models in general according to *CP*, *AW*, and *AWD*, which signifies that IMOWCA has a better capability to optimize the devised system than the original MOWCA. For example, the average *CP* value of the proposed Modes-IMOWCA-CC-MIMOLSSVM model reflects a 5.92% and 1.75% improvement when the interval width coefficient is 0.1 and 0.2, respectively, as compared to the benchmark model Modes-MOWCA-CC-MIMOLSSVM. Furthermore, the average *AWD* value of the proposed model reflects a 0.0310 and 0.0081 improvement as compared to the benchmark model when the interval width coefficient is 0.1 and 0.2, respectively.
(2) The proposal that mode components should be used to interval prediction in the devised system is a significant contribution of this study, since this is the first time mode components have been applied to the interval prediction of wind speed. As compared to the benchmark model IMOWCA-CC-MIMOLSSVM, which does not consider mode components, the comprehensive performance of the devised forecast module is superior to that of the other benchmark models, which illustrates the effectiveness and accuracy of the

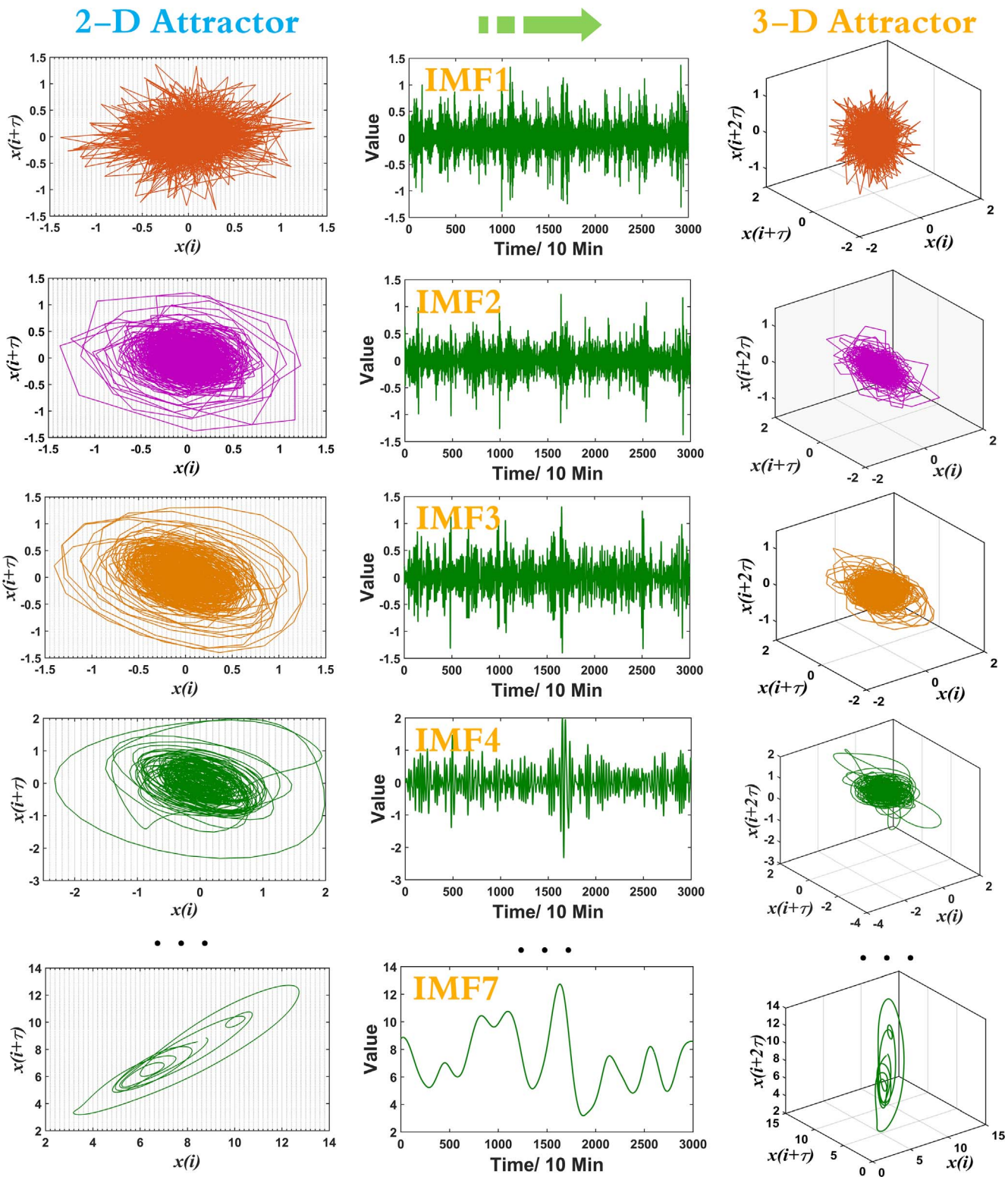

Fig. 6. Attractor of each intrinsic mode function based on Penglai site 1.

system. In summary, the experimental results in Tables 11 and 12 shows that the average *CP* value of the proposed forecast system reflects a 20.28% and 8.40% improvement as compared to the benchmark model IMOWCA-CC-MIMOLSSVM when the interval width coefficient is 0.1 and 0.2, respectively. Furthermore, the average *AWD* value of the proposed forecast module reflects a 0.1120 and 0.0153 improvement as compared to the benchmark model when the interval coefficient is 0.1 and 0.2, respectively.

(3) The C–C method is an excellent means of performing the feature selection in the forecast module, which can enhance the robustness and accuracy of the devised forecast module. As seen in Tables 11 and 12, the average *CP* value of the proposed forecast module reflects a 21.24% and 9.97% improvement as compared to the benchmark model IMOWCA-MIMOLSSVM when the interval width coefficient is 0.1 and 0.2, respectively. Furthermore, the average *AWD* value of the proposed forecast module also reflects a 0.1350

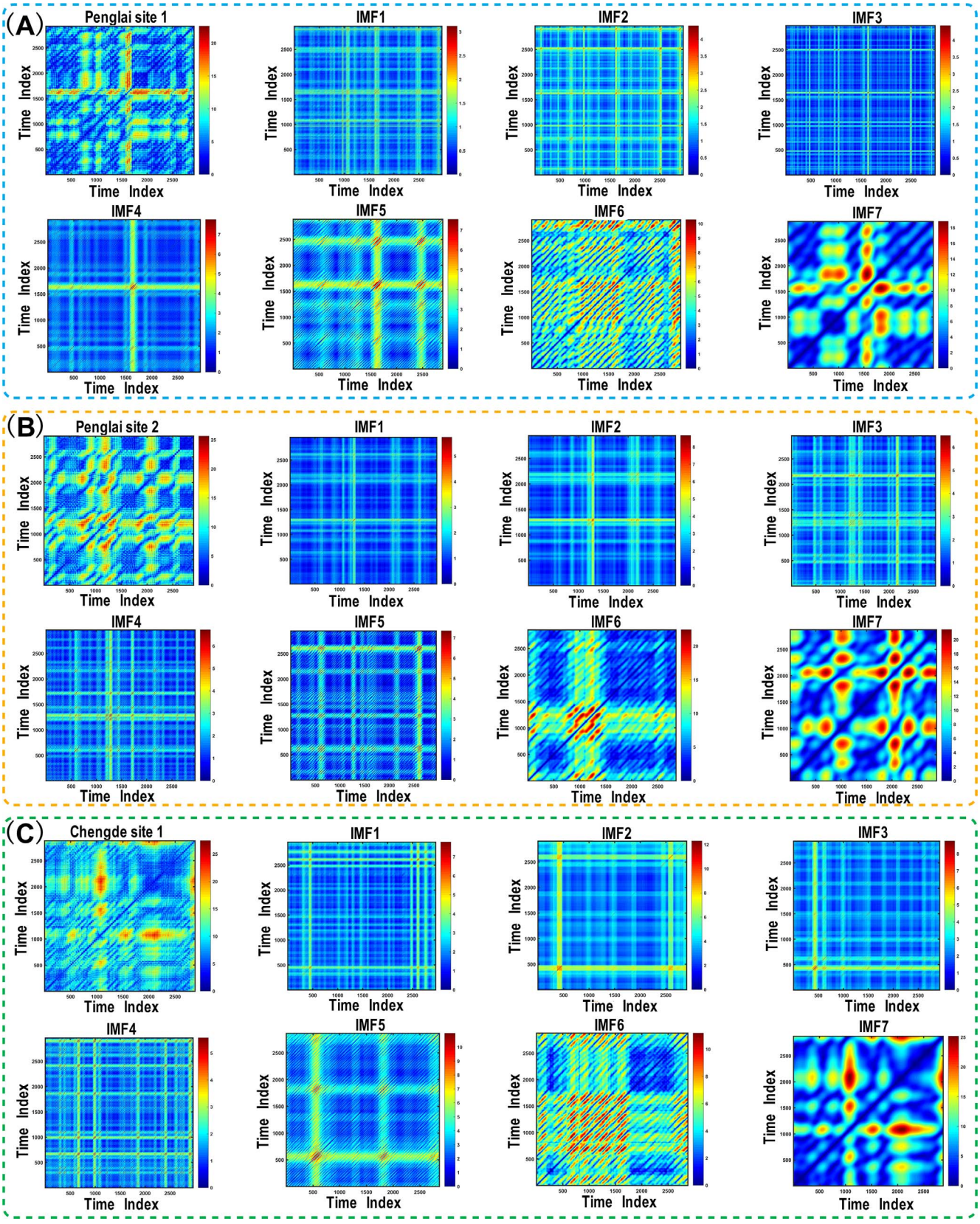

Fig. 7. Frequency-evolving recurrence plots of wind speed series.

improvement when the interval width coefficient is 0.1, and a 0.0294 improvement when the interval width coefficient is 0.2 as compared to the benchmark model. Accordingly, the effective application of the C−C method to interval prediction of wind speed can be considered a contribution of this study.

(4) The performance and effectiveness of the system in the experiments based on Chengde site 1 are inferior to those based on the Penglai sites according to the metrics shown in Tables 11 and 12, which

Table 9
Results of recurrence quantification analysis based on mode components.

Indexes	Original data	IMF1	IMF2	IMF3	IMF4	IMF5	IMF6	IMF7
	Penglai site 1							
Threshold	1.41208	0.13248	0.11221	0.14394	0.20842	0.29988	0.71159	0.97515
RR	0.23898	0.00000	0.00000	0.00000	0.00000	0.00049	0.01493	0.13431
DET	0.93958	0.00000	0.00000	0.00000	0.00000	0.99853	0.99971	1.00000
ENTR	2.10174	0.00000	0.00000	0.00000	0.00000	2.81186	3.79254	5.84611
L	8.10338	–	–	–	–	23.36782	30.00095	192.73229
	Penglai site 2							
Threshold	1.62684	0.16769	0.14856	0.17938	0.24270	0.32118	0.97036	0.98592
RR	0.22655	0.00000	0.00000	0.00000	0.00001	0.00242	0.02594	0.08798
DET	0.94656	0.00000	0.00000	0.00000	0.88462	0.94140	0.99995	0.99999
ENTR	2.15867	0.00000	0.00000	0.00000	1.01865	1.61122	4.63665	5.49362
L	8.94314	–	–	–	2.87500	5.31190	58.46863	134.47020
	Chengde site 1							
Threshold	1.52034	0.24034	0.18110	0.18628	0.22991	0.35677	0.72102	1.08644
RR	0.08488	0.00000	0.00000	0.00000	0.00000	0.00290	0.00594	0.11729
DET	0.79644	0.00000	0.00000	0.00000	0.75000	0.94747	0.99992	0.99999
ENTR	1.26356	0.00000	0.00000	0.00000	0.64111	1.58960	3.71065	5.33671
L	4.08779	–	–	–	2.25000	5.41086	66.42700	118.27968

Table 10
Parameter settings of improved multi-objective water cycle algorithm.

Parameter configuration	Default value
Dimension of the problem	4
Population size	50
Range of population	$[e^{-5}, 1000]$
Size of archive	50
Initial value of inertia weight	0.9
Terminal value of inertia weight	0.45
Number of streams	46
Maximum iteration number	5
Evaporation condition constant	10^{-6}
Number of objectives	2

precisely verifies the remark in the section on uncertainty analysis. Consequently, it is necessary to perform uncertainty analysis of wind speed series, which can provide more information about their predictability, before the interval prediction of wind speed.

(5) Figs. 8–10 show that the prediction intervals yielded by the proposed forecast module are more accurate than those of the benchmark models, because the prediction intervals can cover true wind speed observations with a higher probability. Additionally, the constructed prediction intervals are smoother than those of the benchmark models, indicating that the robustness of the proposed prediction module is more stable.

(6) The results of the devised forecast module shows the same superiority when the experiments were conducted based on data from different wind farms, which further verifies the robustness and effectiveness of the devised system.

Remark. The results of the experiments based on the data from different wind farms significantly testify to the advantages of the proposed forecast module on balance as compared to the benchmark models considered in this study.

5. Further discussion

In this section, the sensitivity analysis concerning iterations of IMOWCA is discussed based on different iteration numbers. Then, the practical significance and the applications of the proposed analysis-

Table 11
Testing results of system performance based on Penglai sites.

Sites	Modes-IMOWCA-CC-MIMOLSSVM				Modes-MOWCA-CC-MIMOLSSVM		
Site 1	*α*	*AW*	*CP*	*AWD*	*AW*	*CP*	*AWD*
	0.1	1.4066	94.01%	0.0193	1.4064	82.40%	0.054
	0.2	2.8001	96.25%	0.0314	2.8230	98.88%	0.0041
	IMOWCA-CC-MIMOLSSVM				IMOWCA-MIMOLSSVM		
	α	*AW*	*CP*	*AWD*	*AW*	*CP*	*AWD*
	0.1	1.3379	71.08%	0.1361	1.3281	72.34%	0.1066
	0.2	2.6675	92%	0.0210	2.6428	92.13%	0.0341
Site 2	Modes-IMOWCA-CC-MIMOLSSVM				Modes-MOWCA-CC-MIMOLSSVM		
	α	*AW*	*CP*	*AWD*	*AW*	*CP*	*AWD*
	0.1	0.9422	81.53%	0.1202	1.1181	80.32%	0.1753
	0.2	2.1944	99.50%	0.0013	2.1845	99.20%	0.0014
	IMOWCA-CC-MIMOLSSVM				IMOWCA-MIMOLSSVM		
	α	*AW*	*CP*	*AWD*	*AW*	*CP*	*AWD*
	0.1	1.0904	69%	0.1372	1.1824	66.24%	0.1949
	0.2	2.1770	89.67%	0.0206	2.3530	86.55%	0.0372

Table 12
Testing results of system performance based on Chengde site 1.

Site	Modes-IMOWCA-CC-MIMOLSSVM				Modes-MOWCA-CC-MIMOLSSVM		
	α	*AW*	*CP*	*AWD*	*AW*	*CP*	*AWD*
Site 1	0.1	1.9488	78.79%	0.0656	1.9652	73.86%	0.0689
	0.2	3.9557	93.56%	0.0229	3.9481	85.98%	0.0744
	IMOWCA-CC-MIMOLSSVM				IMOWCA-MIMOLSSVM		
	α	*AW*	*CP*	*AWD*	*AW*	*CP*	*AWD*
	0.1	1.9122	53.41%	0.2677	1.7203	52.03%	0.3085
	0.2	3.8426	82.44%	0.0599	3.4371	80.71%	0.0726

forecast system are also discussed. Finally, future research directions of interval prediction are suggested.

5.1. Sensitivity analysis on iterations

The iterations of a multi-objective optimization algorithm significantly affect the effectiveness and robustness of uncertainty modeling. An excessive number of iterations may yield over-fitting or fall into local optimum. Accordingly, the algorithm iterations of IMOWCA are discussed based on the wind speed series from Penglai site 1. The simulation results are displayed in Table 13, from which the following conclusions can be drawn.

(1) With an increase in the number of iterations, the metric *AW* shows a trend of fluctuations in different iterations, tending first to increase and then to decrease. The metric *CP* displays a roughly decreasing tendency, which also reveals that the accuracy and effectiveness of the devised model is declining. The metric *AWD* shows a tendency to increase with an increase in iterations, which indicates that the average number of forecasting errors is increasing.
(2) In fact, the different scenarios of uncertainty modeling rely largely on the practical decision-making process. However, considering the performance and computational burden of the devised system, five can be considered a relatively optimal number of iterations on balance.

5.2. Practical significance and Implications of the proposed system

The results of forecasting wind speed, especially of point forecasting, will inevitably produce some bias because of the high randomness of wind speed, which will have a negative influence on the robust scheduling and management of wind power systems in a wind farm. However, effective interval prediction is conducive to mitigating this negative influence. The amount of wind power generated is directly dependent on the wind speed; the formula for the conversion of wind speed to wind power is provided in [85]. In general, effective and comprehensive wind speed forecasting, which plays a major role in maintaining the stability of the wind power system further [49] and

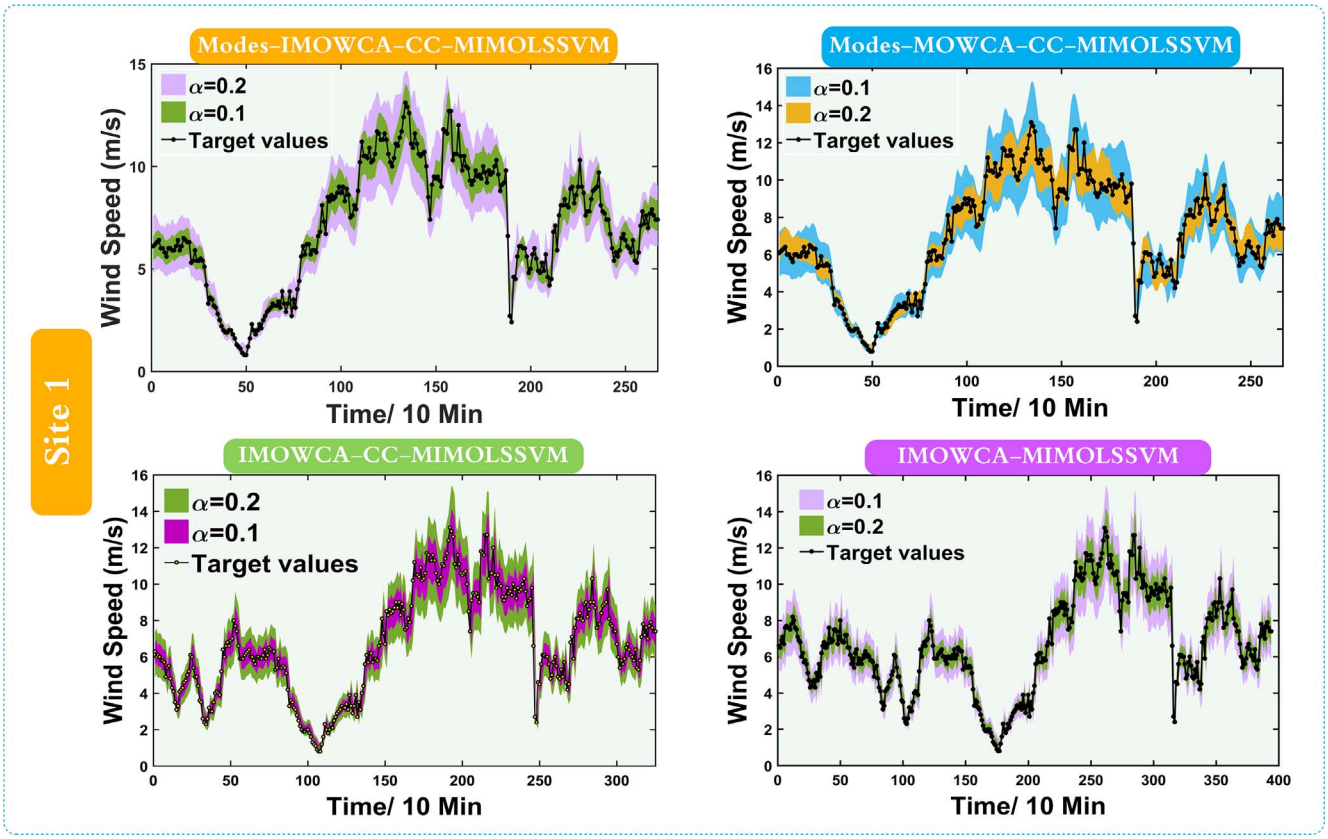

Fig. 8. Visualization of prediction intervals based on Penglai site 1.

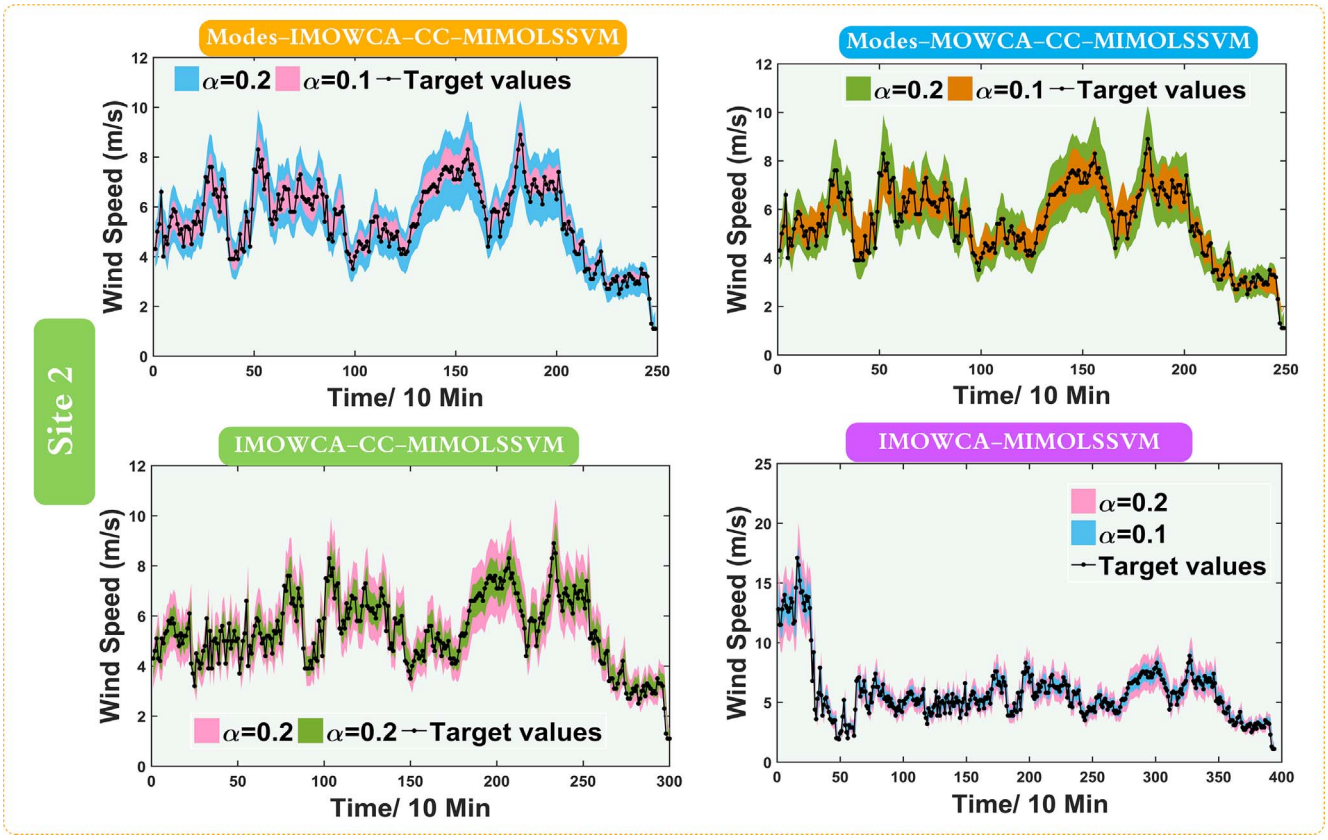

Fig. 9. Visualization of prediction intervals based on Penglai site 2.

improving the efficiency of wind power generation, is urgently needed. Currently, most wind farms focus mainly on point forecasting. However, the investigation and application of interval prediction for wind speed has not received major attention.

As a complement to the current wind power system, the proposed wind speed analysis-forecast system, aimed at providing effective prediction intervals, has great potential to be integrated into the data platform in a wind farm to allow better operation and scheduling of the wind power systems.

Additionally, accurate wind speed forecasting is needed in an effective assessment of wind power, because wind energy is directly proportional to the cube of wind speed and the assessment of potential wind capacity depends ultimately on robust wind speed forecasting.

Although the proposed analysis-forecast system shows a good performance in the uncertainty modeling of wind speed, there remain aspects of this system that need further improvement, which can be summarized as follows.

(1) The proposed analysis-forecast system is focused mainly on short-term interval prediction of wind speed. More effort can be invested in long-term interval prediction of wind speed to further improve the efficiency of operation and scheduling in a wind power system.
(2) In the preprocessing module of the analysis-forecast system, CEEMDAN was developed to refine the wind speed series. However, thus far no perfect theory exists that can help effectively determine the number of IMFs when using CEEMDAN. In the system, the number of IMFs in CEEMDAN was determined by empirical studies. Accordingly, the effective determination of the appropriate number of IMFs when developing wind speed forecasting should be investigated in future studies.

5.3. Future scope

In this study, a comprehensive analysis-forecast system including uncertainty analysis and mining of wind speed was developed. In order to effectively quantify the uncertainty existing in a nonlinear system based on wind speed, the development of new orientations aimed at uncertainty analysis and mining is very necessary. More extensive explorations and investigations in the field should be conducted. Some research directions that should be considered are as follows.

(1) Technically, the physical models based on numerical weather prediction have an advantage in long-term forecasting. Accordingly, combining the physics models and statistical models to perform uncertainty modeling is a not only worthwhile, but also promising direction.
(2) The evaluation metrics of interval prediction should be further investigated in extensive research studies in order to allow a more effective evaluation of the interval prediction models.
(3) In recent years, dynamic multi-objective optimization algorithms have been receiving considerable attention in extensive studies because of their excellent capability for solving dynamic optimization problems. The uncertainty modeling of wind speed in practice usually involves a dynamic and complex environment. Accordingly, the application of dynamic multi-objective optimization algorithms to the field of wind speed or wind power forecasting appears to be a promising research direction.
(4) Deep learning models, as an emerging technology, have been applied to many fields recently. However, the development and application of deep learning techniques to perform uncertainty modeling has rarely received attention, and thus, constitutes a promising research direction.

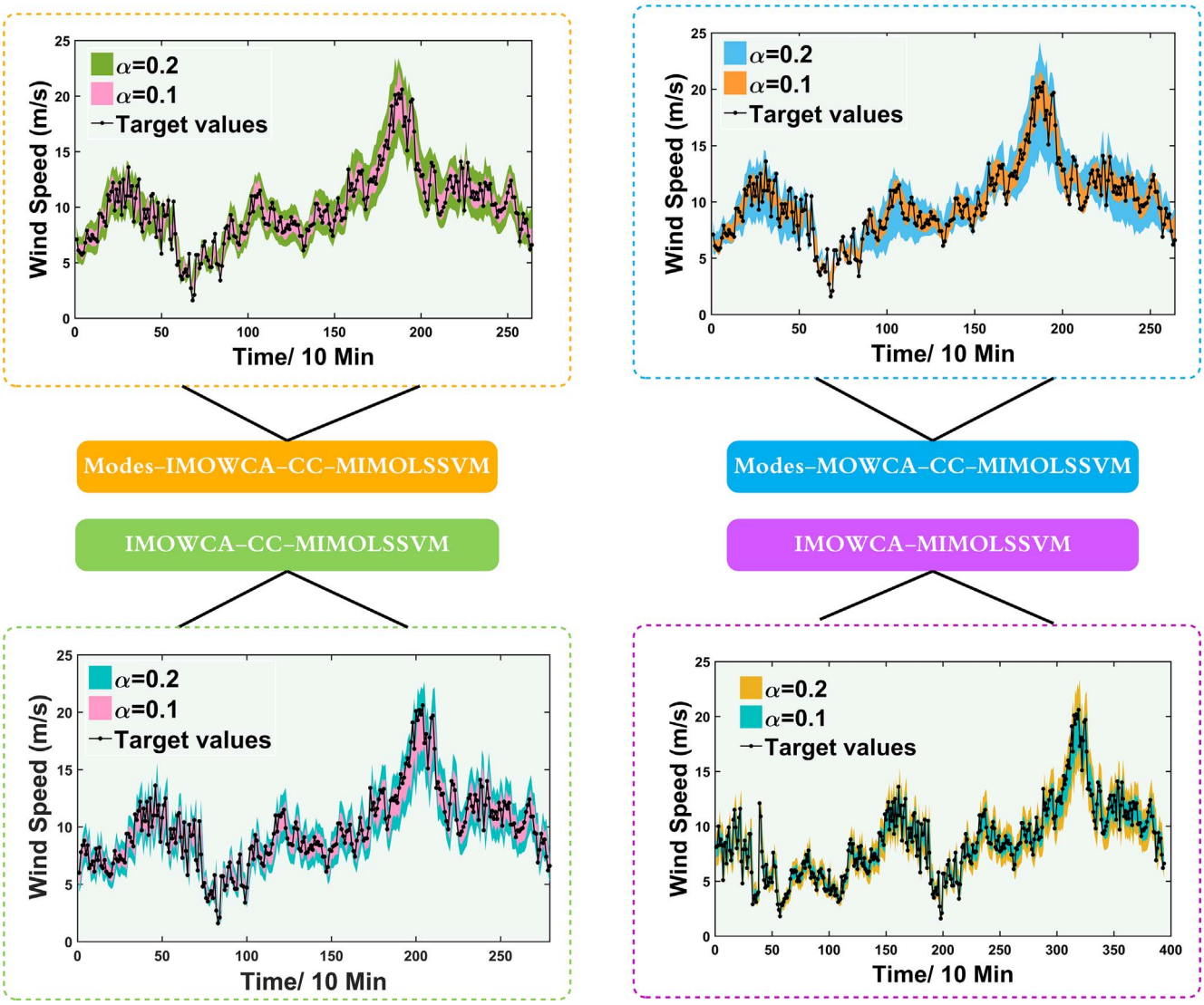

Fig. 10. Visualization of prediction intervals based on Chengde site 1.

Table 13
Sensitivity analysis of different iterations based on improved multi-objective water cycle algorithm.

α	Iteration	*AW*	*CP*	*AWD*
0.1	5	1.4066	94.01%	0.0193
	10	1.4144	86.89%	0.1125
	30	1.4052	88.39%	0.0185
	60	1.4289	49.44%	2.6442
	100	1.4295	19.85%	5.2260
	150	1.3802	46.44%	0.8631
	200	1.3678	72.28%	0.6253
0.2	5	2.8001	96.25%	0.0314
	10	2.8279	96.15%	0.0031
	30	2.7265	71.91%	0.2891
	60	2.7211	73.03%	3.2407
	100	2.8226	44.94%	0.5238
	150	2.7060	64.79%	0.2250
	200	2.7357	72.28%	0.6268

6. Conclusions

With the exhaustion of traditional energy, wind energy is consistently being evaluated worldwide as a promising alternative because of its sustainability and cleanness. However, the further development of wind energy is significantly restricted because of its inherent intermittency and randomness, which possibly put the operation and scheduling of wind farms at risk. In order to more effectively analyze and mine the uncertainty of wind speed, recurrence analysis based on chaos techniques was developed in this study to reveal the inherent dynamic characteristics of wind speed, which is vital for exploring the predictability and modeling of the uncertainty of wind speed. Furthermore, an effective forecast module integrating mode components, chaos techniques, and IMOWCA was successfully devised. Importantly, mode components (or frequency domains) were developed for the first time to perform uncertainty modeling, which was proved to be significantly more effective and robust than the benchmark models considered in this study. Furthermore, MOWCA was further developed by introducing the adaptive inertia weight, leading to a novel multi-objective algorithm, namely, IMOWCA. The results of numerical experiments to test the algorithm clearly illustrate that IMOWCA is a significant improvement on the original MOWCA on balance. Finally, extensive experiments using quantitative metrics revealed the significant effectiveness and superiority of the system in this study. Additionally, given the excellent performance of the devised system, it can also be applied in practice in the fields of load forecasting, wind power forecasting, and stock forecasting, and so forth.

Conflict of interests

The authors declare that there is no conflict of interests regarding the publication of this paper.

Acknowledgements

This research was supported by the National Natural Science Foundation of China (Grant No. 71671029 and Grant No. 41475013).

Appendix A

Multi-objective test functions used in this paper (see Table A).

Table A
Testing problems.

Problem	Dimension	Range	Expression	Continuity	Convexity
ZDT1	30	[0, 1]	$\boldsymbol{Minimize} = \begin{cases} f_1(x) = x_1 \\ f_2(x) = g(x) \times \boldsymbol{h}(f_1(x), g(x)) \\ g(x) = 1 + \frac{9}{29}\sum_{i=2}^{30} x_i \\ \boldsymbol{h}(f_1(x), g(x)) = 1 - \sqrt{\frac{f_1(x)}{g(x)}} \end{cases}$	✓	✓
ZDT3	30	[0, 1]	$\boldsymbol{Minimize} = \begin{cases} f_1(x) = x_1 \\ f_2(x) = g(x) \times \boldsymbol{h}(f_1(x), g(x)) \\ g(x) = 1 + \frac{9}{29}\sum_{i=2}^{30} x_i \\ \boldsymbol{h}(f_1(x), g(x)) = 1 - \sqrt{\frac{f_1(x)}{g(x)}} - (\frac{f_1(x)}{g(x)}) \times \sin(10\pi f_1(x)) \end{cases}$	✗	✓
Kursawe	3	[−5, 5]	$\boldsymbol{Minimize} = \begin{cases} f_1(x) = \sum_{i=1}^{2} [-10\exp(-0.2\sqrt{x_i^2 + x_{i+1}^2})] \\ f_2(x) = \sum_{i=1}^{3} [\lvert x_i \rvert^{0.8} + 5\sin(x_i^3)] \end{cases}$	✗	✗
Viennet3	2	[−3, 3]	$\boldsymbol{Minimize} = \begin{cases} f_1(x,y) = 0.5(x^2 + y^2) + \sin(x^2 + y^2) \\ f_2(x,y) = \frac{(3x - 2y + 4)^2}{8} + \frac{(x - y + 1)^2}{27} + 15 \\ f_3(x,y) = \frac{1}{(x^2 + y^2 + 1)} - 1.1\exp(-x^2 - y^2) \end{cases}$	✓	–

References

[1] Pourbeik P, Akhmatov V, Akiyama Y, et al. Modelling and dynamic behavior of wind generation as it relates to power system control and dynamic performance[J] 2007.

[2] Yu J, Ji F, Zhang L, Chen Y. An over painted oriental arts: evaluation of the development of the Chinese renewable energy market using the wind power market as a model. Energy Policy 2009;37:5221–5. http://dx.doi.org/10.1016/j.enpol.2009.07.035.

[3] Wang Y, Wang J, Wei X. A hybrid wind speed forecasting model based on phase space reconstruction theory and Markov model: a case study of wind farms in northwest China. Energy 2015;91:556–72. http://dx.doi.org/10.1016/j.energy.2015.08.039.

[4] Baseer MA, Meyer JP, Rehman S, Mahbub AM, Al-Hadhrami LM, Lashin A. Performance evaluation of cup-anemometers and wind speed characteristics analysis. Renew Energy 2016;86:733–44. http://dx.doi.org/10.1016/j.renene.2015.08.062.

[5] Santamaría-Bonfil G, Reyes-Ballesteros A, Gershenson C. Wind speed forecasting for wind farms: a method based on support vector regression. Renew Energy 2016;85:790–809. http://dx.doi.org/10.1016/j.renene.2015.07.004.

[6] Wang J, Qin S, Zhou Q, Jiang H. Medium-term wind speeds forecasting utilizing hybrid models for three different sites in Xinjiangm, China. Renew Energy 2015;76:91–101. http://dx.doi.org/10.1016/j.renene.2014.11.011.

[7] Hu Q, Zhang R, Zhou Y. Transfer learning for short-term wind speed prediction with deep neural networks. Renew Energy 2016;85:83–95. http://dx.doi.org/10.1016/j.renene.2015.06.034.

[8] Telesca L, Lovallo M, Kanevski M. Power spectrum and multifractal detrended fluctuation analysis of high-frequency wind measurements in mountainous regions. Appl Energy 2016;162:1052–61. http://dx.doi.org/10.1016/j.apenergy.2015.10.187.

[9] Bigdeli N, Afshar K, Gazafroudi AS, Ramandi MY. A comparative study of optimal hybrid methods for wind power prediction in wind farm of Alberta. Canada. Renew Sustain Energy Rev 2013;27:20–9. http://dx.doi.org/10.1016/j.rser.2013.06.022.

[10] Yu YSW, Sun D, Zhang J, Xu Y, Qi Y. Study on a Pi-type mean flow acoustic engine capable of wind energy harvesting using a CFD model. Appl Energy 2017;189:602–12. http://dx.doi.org/10.1016/j.apenergy.2016.12.022.

[11] Sun D, Xu Y, Chen H, Wu K, Liu K, Yu Y. A mean flow acoustic engine capable of wind energy harvesting. Energy Convers Manage 2012;63:101–5. http://dx.doi.org/10.1016/j.enconman.2011.12.035.

[12] Yu Y, Sun D, Wu K, Xu Y, Chen H, Zhang X, et al. CFD study on mean flow engine for wind power exploitation. Energy Convers Manage 2011;52:2355–9. http://dx.doi.org/10.1016/j.enconman.2010.12.046.

[13] Jung J, Broadwater RP. Current status and future advances for wind speed and power forecasting. Renew Sustain Energy Rev 2014;31:762–77. http://dx.doi.org/10.1016/j.rser.2013.12.054.

[14] Zhao J, Guo Z-H, Su Z-Y, Zhao Z-Y, Xiao X, Liu F. An improved multi-step forecasting model based on WRF ensembles and creative fuzzy systems for wind speed. Appl Energy 2016;162:808–26. http://dx.doi.org/10.1016/j.apenergy.2015.10.145.

[15] Lei M, Shiyan L, Chuanwen J, Hongling L, Yan Z. A review on the forecasting of wind speed and generated power. Renew Sustain Energy Rev 2009;13:915–20. http://dx.doi.org/10.1016/j.rser.2008.02.002.

[16] Costa A, Crespo A, Navarro J, Lizcano G, Madsen H, Feitosa E. A review on the young history of the wind power short-term prediction. Renew Sustain Energy Rev 2008;12:1725–44. http://dx.doi.org/10.1016/j.rser.2007.01.015.

[17] Landberg L, Giebel G, Nielsen HA, Nielsen T, Madsen H. Short-term prediction – an overview. Wind Energy 2003;6:273–80. http://dx.doi.org/10.1002/we.96.

[18] Cassola F, Burlando M. Wind speed and wind energy forecast through Kalman filtering of Numerical Weather Prediction model output. Appl Energy 2012;99:154–66. http://dx.doi.org/10.1016/j.apenergy.2012.03.054.

[19] Poggi P, Muselli M, Notton G, Cristofari C, Louche A. Forecasting and simulating wind speed in Corsica by using an autoregressive model. Energy Convers Manage 2003;44:3177–96. http://dx.doi.org/10.1016/S0196-8904(03)00108-0.

[20] Erdem E, Shi J. ARMA based approaches for forecasting the tuple of wind speed and direction. Appl Energy 2011;88:1405–14. http://dx.doi.org/10.1016/j.apenergy.2010.10.031.

[21] Torres JL, García A, De Blas M, De Francisco A. Forecast of hourly average wind speed with ARMA models in Navarre (Spain). Sol Energy 2005;79:65–77. http://dx.doi.org/10.1016/j.solener.2004.09.013.

[22] Kavasseri RG, Seetharaman K. Day-ahead wind speed forecasting using f-ARIMA models. Renew Energy 2009;34:1388–93. http://dx.doi.org/10.1016/j.renene.2008.09.006.

[23] Wang M Di, Qiu QR, Cui BW. Short-term wind speed forecasting combined time series method and arch model. Proc. – Int. Conf. Mach. Learn. Cybern. vol. 3, 2012, p. 924–7. doi:10.1109/ICMLC.2012.6359477.

[24] Cadenas E, Rivera W. Short term wind speed forecasting in La Venta, Oaxaca, Mexico, using artificial neural networks. Renew Energy 2009;34:274–8.

[25] Guo Z, Wu J, Lu H, Wang J. A case study on a hybrid wind speed forecasting method using BP neural network. Knowledge-Based Syst 2011;24:1048–56. http://dx.doi.org/10.1016/j.knosys.2011.04.019.

[26] Monfared M, Rastegar H, Kojabadi HM. A new strategy for wind speed forecasting using artificial intelligent methods. Renew Energy 2009;34:845–8. http://dx.doi.org/10.1016/j.renene.2008.04.017.

[27] Guo Z, Zhao W, Lu H, Wang J. Multi-step forecasting for wind speed using a modified EMD-based artificial neural network model. Renew Energy

2012;37:241–9. http://dx.doi.org/10.1016/j.renene.2011.06.023.
[28] Liu H, Tian H, Liang X, Li Y. Wind speed forecasting approach using secondary decomposition algorithm and Elman neural networks. Appl Energy 2015;157:183–94. http://dx.doi.org/10.1016/j.apenergy.2015.08.014.
[29] Zhang W, Qu Z, Zhang K, Mao W, Ma Y, Fan X. A combined model based on CEEMDAN and modified flower pollination algorithm for wind speed forecasting. Energy Convers Manage 2017;136:439–51. http://dx.doi.org/10.1016/j.enconman.2017.01.022.
[30] Zhang Y, Liu K, Qin L, An X. Deterministic and probabilistic interval prediction for short-term wind power generation based on variational mode decomposition and machine learning methods. Energy Convers Manage 2016;112:208–19. http://dx.doi.org/10.1016/j.enconman.2016.01.023.
[31] Liu H, Tian HQ, Chen C, Li YF. An experimental investigation of two wavelet-MLP hybrid frameworks for wind speed prediction using GA and PSO optimization. Int J Electr Power Energy Syst 2013;52:161–73. http://dx.doi.org/10.1016/j.ijepes.2013.03.034.
[32] Su Z, Wang J, Lu H, Zhao G. A new hybrid model optimized by an intelligent optimization algorithm for wind speed forecasting. Energy Convers Manage 2014;85:443–52. http://dx.doi.org/10.1016/j.enconman.2014.05.058.
[33] Wang S, Zhang N, Wu L, Wang Y. Wind speed forecasting based on the hybrid ensemble empirical mode decomposition and GA-BP neural network method. Renew Energy 2016;94:629–36. http://dx.doi.org/10.1016/j.renene.2016.03.103.
[34] Liu H, Tian H, Liang X, Li Y. New wind speed forecasting approaches using fast ensemble empirical model decomposition, genetic algorithm, Mind Evolutionary Algorithm and Artificial Neural Networks. Renew Energy 2015;83:1066–75. http://dx.doi.org/10.1016/j.renene.2015.06.004.
[35] Liu D, Niu D, Wang H, Fan L. Short-term wind speed forecasting using wavelet transform and support vector machines optimized by genetic algorithm. Renew Energy 2014;62:592–7. http://dx.doi.org/10.1016/j.renene.2013.08.011.
[36] Catalao JPS, Pousinho HMI, Mendes VMF. Hybrid wavelet-PSO-ANFIS approach for short-termwind power forecasting in Portugal. IEEE Trans Sustain Energy 2010;2:50–9. http://dx.doi.org/10.1109/TSTE.2010.2076359.
[37] Yang L, He M, Zhang J, Vittal V. Support-vector-machine-enhanced markov model for short-term wind power forecast. IEEE Trans Sustain Energy 2015;6:791–9. http://dx.doi.org/10.1109/TSTE.2015.2406814.
[38] Lahouar A, Ben Hadj Slama J. Hour-ahead wind power forecast based on random forests. Renew Energy 2017;109:529–41. http://dx.doi.org/10.1016/j.renene.2017.03.064.
[39] Zhao Y, Ye L, Li Z, Song X, Lang Y, Su J. A novel bidirectional mechanism based on time series model for wind power forecasting. Appl Energy 2016;177:793–803. http://dx.doi.org/10.1016/j.apenergy.2016.03.096.
[40] Dong Q, Sun Y, Li P. A novel forecasting model based on a hybrid processing strategy and an optimized local linear fuzzy neural network to make wind power forecasting: a case study of wind farms in China. Renew Energy 2017;102:241–57. http://dx.doi.org/10.1016/j.renene.2016.10.030.
[41] Sideratos G, Hatziargyriou ND. Probabilistic wind power forecasting using radial basis function neural networks. IEEE Trans Power Syst 2012;27:1788–96. http://dx.doi.org/10.1109/TPWRS.2012.2187803.
[42] Chitsaz H, Amjady N, Zareipour H. Wind power forecast using wavelet neural network trained by improved Clonal selection algorithm. Energy Convers Manage 2015;89:588–98. http://dx.doi.org/10.1016/j.enconman.2014.10.001.
[43] Wang HZ, Wang GB, Li GQ, Peng JC, Liu YT. Deep belief network based deterministic and probabilistic wind speed forecasting approach. Appl Energy 2016;182:80–93. http://dx.doi.org/10.1016/j.apenergy.2016.08.108.
[44] Bremnes JB. Probabilistic wind power forecasts using local quantile regression. Wind Energy 2004;7:47–54. http://dx.doi.org/10.1002/we.107.
[45] Nielsen HA, Madsen H, Nielsen TS. Using quanti le regression to extend an existing wind power forecasting system with probabilistic forecasts. Wind Energy 2006;9:95–108. http://dx.doi.org/10.1002/we.180.
[46] Errouissi R, Cardenas-Barrera J, Meng J, Castillo-Guerra E, Gong X, Chang L. Bootstrap prediction interval estimation for wind speed forecasting. 2015 IEEE Energy Convers. Congr. Expo. ECCE 2015, 2015, p. 1919–24. doi: 10.1109/ECCE.2015.7309931.
[47] Juban J, Siebert N, Kariniotakis GN. Probabilistic short-term wind power forecasting for the optimal management of wind generation. IEEE Lausanne Power Tech 2007;2007:683–8. http://dx.doi.org/10.1109/PCT.2007.4538398.
[48] Khosravi A, Nahavandi S, Creighton D, Atiya AF. Lower upper bound estimation method for construction of neural network-based prediction intervals. IEEE Trans Neural Networks 2011;22:337–46. http://dx.doi.org/10.1109/TNN.2010.2096824.
[49] Yan J, Liu Y, Han S, Wang Y, Feng S. Reviews on uncertainty analysis of wind power forecasting. Renew Sustain Energy Rev 2015;52:1322–30. http://dx.doi.org/10.1016/j.rser.2015.07.197.
[50] Bootstrapping and Resampling. < http://www.ncl.ucar.edu/Applications/bootstrap.shtml > .
[51] Yeh J-R, Shieh J-S, Huang NE. Complementary ensemble empirical mode decomposition: a novel noise enhanced data analysis method. Adv Adapt Data Anal 2010;02:135–56. http://dx.doi.org/10.1142/S1793536910000422.
[52] Torres ME, Colominas MA, Schlotthauer G, Flandrin P. A complete ensemble empirical mode decomposition with adaptive noise. 2011 IEEE Int Conf Acoust Speech Signal Process 2011;7:4144–7. doi: 10.1109/ICASSP.2011.5947265.
[53] Huang NE, Shen Z, Long SR, Wu MC, Shih HH, Zheng Q, et al. The empirical mode decomposition and the Hilbert spectrum for nonlinear and non-stationary time series analysis. Proc R Soc A Math Phys Eng Sci 1998;454:903–95. http://dx.doi.org/10.1098/rspa.1998.0193.
[54] Wu Z, Huang NE. Ensemble empirical mode decomposition: a noise-assisted data analysis method. Adv Adapt Data Anal 2009;01:1–41. http://dx.doi.org/10.1142/S1793536909000047.
[55] Marwan N, Carmen Romano M, Thiel M, Kurths J. Recurrence plots for the analysis of complex systems. Phys Rep 2007;438:237–329. http://dx.doi.org/10.1016/j.physrep.2006.11.001.
[56] Eckmann JP, Kamphorst SO, Ruelle D, Ciliberto S. Liapunov exponents from time series. Phys Rev A 1986;34:4971–9. http://dx.doi.org/10.1103/PhysRevA.34.4971.
[57] Marwan N, Wessel N, Meyerfeldt U, Schirdewan A, Kurths J. Recurrence-plot-based measures of complexity and their application to heart-rate-variability data. Phys Rev E – Stat Nonlinear, Soft Matter Phys 2002;66. http://dx.doi.org/10.1103/PhysRevE.66.026702.
[58] Zbilut JP, Webber CL. Embeddings and delays as derived from quantification of recurrence plots. Phys Lett A 1992;171:199–203. http://dx.doi.org/10.1016/0375-9601(92)90426-M.
[59] Webber CL, Zbilut JP. Dynamical assessment of physiological systems and states using recurrence plot strategies. J Appl Physiol 1994;76:965–73.
[60] Kim HS, Eykholt R, Salas JD. Nonlinear dynamics, delay times, and embedding windows. Phys D Nonlinear Phenom 1999;127:48–60. http://dx.doi.org/10.1016/S0167-2789(98)00240-1.
[61] Carbonneau R, Laframboise K, Vahidov R. Application of machine learning techniques for supply chain demand forecasting. Eur J Oper Res 2008;184:1140–54. http://dx.doi.org/10.1016/j.ejor.2006.12.004.
[62] Vapnik VN. The nature of statistical learning theory. Springer 1995;8:188. doi: 10.1109/TNN.1997.641482.
[63] Bouhouche S, Laksir Yazid L, Hocine S, Bast J. Evaluation using online support-vector-machines and fuzzy reasoning. Application to condition monitoring of speeds rolling process. Control Eng Pract 2010;18:1060–8. http://dx.doi.org/10.1016/j.conengprac.2010.05.010.
[64] Wang JZ, Wang Y, Jiang P. The study and application of a novel hybrid forecasting model – a case study of wind speed forecasting in China. Appl Energy 2015;143:472–88. http://dx.doi.org/10.1016/j.apenergy.2015.01.038.
[65] Han Z, Liu Y, Zhao J, Wang W. Real time prediction for converter gas tank levels based on multi-output least square support vector regressor. Control Eng Pract 2012;20:1400–9. http://dx.doi.org/10.1016/j.conengprac.2012.08.006.
[66] Heidari AA, Ali Abbaspour R, Rezaee Jordehi A. Gaussian bare-bones water cycle algorithm for optimal reactive power dispatch in electrical power systems. Appl Soft Comput J 2017;57. http://dx.doi.org/10.1016/j.asoc.2017.04.048.
[67] Sarvi M, Avanaki IN. An optimized fuzzy logic controller by water cycle algorithm for power management of stand-alone hybrid green power generation. Energy Convers Manage 2015;106:118–26. http://dx.doi.org/10.1016/j.enconman.2015.09.021.
[68] Gao K, Zhang Y, Sadollah A, Lentzakis A, Su R. Jaya, harmony search and water cycle algorithms for solving large-scale real-life urban traffic light scheduling problem. Swarm Evol Comput 2016. http://dx.doi.org/10.1016/j.swevo.2017.05.002.
[69] Eskandar H, Sadollah A, Bahreininejad A, Hamdi M. Water cycle algorithm – a novel metaheuristic optimization method for solving constrained engineering optimization problems. Comput Struct 2012;110–111:151–66. http://dx.doi.org/10.1016/j.compstruc.2012.07.010.
[70] Khodabakhshian A, Esmaili MR, Bornapour M. Optimal coordinated design of UPFC and PSS for improving power system performance by using multi-objective water cycle algorithm. Int J Electr Power Energy Syst 2016;83:124–33. http://dx.doi.org/10.1016/j.ijepes.2016.03.052.
[71] Sadollah A, Eskandar H, Kim JH. Water cycle algorithm for solving constrained multi-objective optimization problems. Appl Soft Comput 2015;27:279–98. http://dx.doi.org/10.1016/j.asoc.2014.10.042.
[72] Deihimi A, Keshavarz Zahed B, Iravani R. An interactive operation management of a micro-grid with multiple distributed generations using multi-objective uniform water cycle algorithm. Energy 2016;106:482–509. http://dx.doi.org/10.1016/j.energy.2016.03.048.
[73] Deb K, Pratap A, Agarwal S, Meyarivan T. A fast and elitist multiobjective genetic algorithm: NSGA-II. IEEE Trans Evol Comput 2002;6:182–97. http://dx.doi.org/10.1109/4235.996017.
[74] Zitzler E, Laumanns M, Thiele L. SPEA2: Improving the Strength Pareto Evolutionary Algorithm. Evol Methods Des Optim Control Appl Ind Probl 2001:95–100. 10.1.1.28.7571.
[75] Knowles J, Corne D. The Pareto archived evolution strategy: a new baseline algorithm for Pareto multiobjective optimisation. In: Proc 1999 Congr Evol Comput CEC 1999, vol. 1, 1999, p. 98–105. doi: 10.1109/CEC.1999.781913.
[76] Srinivas N, Deb K. Muiltiobjective optimization using nondominated sorting in genetic algorithms. Evol Comput 1994;2:221–48. http://dx.doi.org/10.1162/evco.1994.2.3.221.
[77] Zitzler E, Thiele L. Multiobjective optimization using evolutionary algorithms – a comparative case study. Proc Int Conf Parallel Probl Solving Nat 1998:292–304. http://dx.doi.org/10.1007/BFb0056872.
[78] Van Veldhuizen Da, Lamont GB. Evolutionary computation and convergence to a pareto front. Late Break Pap Genet Program 1998 Conf 1998:221–8.
[79] Hong YY, Lin JK. Interactive multi-objective active power scheduling considering uncertain renewable energies using adaptive chaos clonal evolutionary programming. Energy 2013;53:212–20. http://dx.doi.org/10.1016/j.energy.2013.02.070.
[80] Schott JR, OH AIRFIOFTW-PAFB. Fault Tolerant Design Using Single and Multicriteria Genetic Algorithm Optimization 1995;37(1):1–13.
[81] Conti S, Nicolosi R, Rizzo SA, Zeineldin HH. Optimal dispatching of distributed generators and storage systems for MV islanded microgrids. IEEE Trans Power Deliv 2012;27:1243–51. http://dx.doi.org/10.1109/TPWRD.2012.2194514.
[82] Wolf A, Swift JB, Swinney HL, Vastano JA. Determining Lyapunov exponents from a time series. Phys D Nonlinear Phenom 1985;16:285–317. http://dx.doi.org/10.1016/0167-2789(85)90011-9.
[83] James G, Witten D, Hastie T, Tibshirani R. An introduction to statistical learning. Economica 2013;103(2):78–129. http://dx.doi.org/10.1007/978-1-4614-7138-7.
[84] Bermingham ML, Pong-Wong R, Spiliopoulou A, Hayward C, Rudan I, Campbell H, et al. Application of high-dimensional feature selection: evaluation for genomic prediction in man. Sci Rep 2015;5:10312. http://dx.doi.org/10.1038/srep10312.
[85] Wang J, Du P, Niu T, Yang W. A novel hybrid system based on a new proposed algorithm—multi-objective whale optimization algorithm for wind speed forecasting. Appl Energy 2017. http://dx.doi.org/10.1016/j.apenergy.2017.10.031.